Physics of the Earth and Planetary Interiors 171 (2008) 235–251

Contents lists available at ScienceDirect

Physics of the Earth and Planetary Interiors

journal homepage: www.elsevier.com/locate/pepi

From passive continental margin to mountain belt: Insights from analytical and numerical models and application to Taiwan

Boris J.P. Kaus[a,b,*], Clare Steedman[b], Thorsten W. Becker[b]

[a] Geophysical Fluid Dynamics, Department of Earth Sciences, ETH Zürich, Schafmattstrasse 30, CH-8093 Zurich, Switzerland
[b] Department of Earth Sciences, University of Southern California, 3651 Trousdale Parkway, Los Angeles, CA-90089-740, USA

ARTICLE INFO

Article history:
Received 28 October 2007
Received in revised form 19 June 2008
Accepted 20 June 2008

Keywords:
Passive continental margin
Subduction
Surface processes
Taiwan
Mantle/lithosphere interaction
Lithosphere deformation
Finite element technique

ABSTRACT

The physics of deformation at plate boundaries is insufficiently understood. Taiwan is particularly interesting in this context since geological and geophysical arguments indicate that passive-margin sediments were exhumed into an active mountain belt over a relatively short period of time. Classically, Taiwan has been described as a critical wedge orogeny, in which deformation is entirely restricted to the crust. More recent data, however, indicate that deeper parts of the lithosphere also participate in deformation. In order to study the physical feasibility of various endmember hypothesis, we have performed two-dimensional (2-D) thermo-mechanical numerical experiments in which both mantle, lithospheric and surface processes are taken into account and in which crustal deformation evolves as a function of mantle flow. Our setup consists of ocean–ocean subduction, followed by passive continental margin deformation.

Results indicate that in most cases the subducting slab becomes close to vertical upon arrival of continental material to the trench. Whereas crustal rheology, deformation and surface processes do not modify mantle flow significantly, they are important for crustal-scale processes. Relatively little crustal exhumation occurs if the crust is homogeneous and erosion rates are small. Significant exhumation in a dome-like structure is obtained if a weak lower crust and large erosion rates are present. The presence of an oceanic arc in the overriding oceanic lithosphere modifies, but does not control, crustal deformation. Synthetic metamorphic facies maps and thermochronological data, computed from the numerical models, are in reasonable agreement with observations in Southern Taiwan if exhumation occurs in a dome-like structure.

Further physical insight in the doming mechanisms is obtained by a combination of analytical techniques and crustal-scale numerical models. This analysis indicates that the dome-like exhumation mechanism can be attributed to a compressional mechanical instability, facilitated by both a weak lower crust and large rates of erosion. Both conditions are likely to be satisfied in Taiwan.

1. Introduction

The dynamics of plate boundaries and in particular the interaction between subduction and mountain belt formation remains one of the more enigmatic problems in tectonics. One of the places on Earth where such process can currently be observed is Taiwan, where an initial ocean–ocean subduction changed into an ocean-continent and continent–ocean subduction, in a fairly complex three-dimensional setting (Suppe, 1984; Lallemand et al., 2001; Malavieille et al., 2002; Sibuet and Hsu, 2004). Taiwan is peculiar in that it has one of the highest erosion rates on Earth, emerged above the sea-level only 5 Myrs ago, and is seismically very active. Not surprisingly, therefore, it has been the focus of many previous and ongoing studies that yielded important constraints on the geology and geophysics of the island (Suppe, 1981; Wu et al., 1997; Willett et al., 2003; Sibuet and Hsu, 2004; Wu, 2007). Many of those studies indicated that mountain belt formation in Taiwan started in the North and migrated southward over a period of $\sim$ 6 Myrs, possibly related to the collision of the Luzon arc with the continental margin (Yen, 1973; Suppe, 1984).

The crustal-scale evolution of Taiwan has been one of the inspirations for the development of orogenic critical wedge models, which assume that deformation is largely restricted to the upper crust. Following the pioneering work of Suppe, Dahlen, and coworkers (Dahlen and Barr, 1989; Barr and Dahlen, 1989; Suppe, 1981, 1987), a number of 2-D thermo-kinematic (Lin, 2000; Simoes et al., 2007; Willett et al., 2003) and thermo-mechanical (Fuller et al., 2006) models have been developed that explained part of the evolution and thermal history of Taiwan. More recently, however, an increasing amount of data indicates that deformation in Taiwan is

* Corresponding author.
E-mail address: kaus@erdw.ethz.ch (B.J.P. Kaus).

0031-9201/$ – see front matter © 2008 Elsevier B.V. All rights reserved.
doi:10.1016/j.pepi.2008.06.015

not just restricted to the upper crust but involves the whole lithosphere (Wu et al., 1997; Gourley et al., 2007). Obtaining insight in the physics of such a system requires models in which mantle deformation is not prescribed kinematically, but in which it can evolve in a self-consistent manner.

Over the last few years, a number of numerical techniques have become available that can study coupled mantle–lithosphere processes (Beaumont et al., 2001; Pysklywec et al., 2002; Sobolev and Babeyko, 2005; Faccenda et al., 2008; Yamato et al., 2007), in a self-consistent manner. The transition from ocean–ocean subduction to passive margin-ocean subduction, as it is of relevance for Taiwan, has not been addressed yet with such models.

In this paper, we therefore focus on the physics of this process, by using a combination of dynamic numerical models and analytical theory. Being two-dimensional, the models cannot address topics related to 3-D plate interaction in the region, previously studied with laboratory experiments (Chemenda et al., 2001). They, however, have the advantage of allowing to study the coupling between mantle scale, lithospheric scale and surface processes in a self-consistent manner, without need for kinematically prescribed boundary conditions.

We start by describing the numerical technique, followed by a parameter study with lithospheric-scale models that yield insight in mantle–lithosphere interaction as well as in the key parameters that affect model behavior. Synthetic metamorphic facies maps as well as cooling rates allow comparisons with observations. The results of the large-scale models are then used to construct simpler models that are studied in a systematic manner with both analytical approaches and numerical simulations. This approach yields insight in the physics of mountain building processes from passive continental margins.

2. Governing equations

On the time- and length-scales relevant for long-term lithospheric processes, inertial terms are negligible and the governing two-dimensional (2-D) force balance equations can be expressed as:

$$-\frac{\partial P}{\partial x}+\frac{\partial \tau_{xx}}{\partial x}+\frac{\partial \tau_{xz}}{\partial z}=0, \tag{1}$$

$$-\frac{\partial P}{\partial z}+\frac{\partial \tau_{xz}}{\partial x}+\frac{\partial \tau_{zz}}{\partial z}=\rho g, \tag{2}$$

where $P=-\sigma_{ii}/3$ is pressure, τ_{xx}, τ_{zz}, τ_{xz} denote deviatoric stresses, ρ density, g gravitational acceleration (acting in z-direction) and x, z horizontal and vertical coordinates respectively. Conservation of mass is given by

$$\dot{\varepsilon}_{xx}+\dot{\varepsilon}_{zz}=-\frac{1}{K}\frac{\partial P}{\partial t}, \tag{3}$$

where $\dot{\varepsilon}_{xx}$, $\dot{\varepsilon}_{zz}$ denote horizontal and vertical strain rates respectively, t is time and K is the elastic bulk modulus of rocks deforming in the elastic regime. If deformation processes are dominated by viscous creep, $K\to\infty$ and deformation is effectively incompressible. Rheology is visco-elasto-plastic

$$\tilde{\dot{\varepsilon}}_{ij}=\frac{1}{2G}\frac{D\tau_{ij}}{Dt}+\frac{1}{2\mu}\tau_{ij}+\dot{\lambda}\frac{\partial Q}{\partial \sigma_{ij}}, \tag{4}$$

where $\dot{\varepsilon}_{ij}=(1/2)((\partial v_i/\partial x_j)+(\partial v_j/\partial x_i))$ is strain rate, v_i velocity, $\tilde{\dot{\varepsilon}}_{ij}=\dot{\varepsilon}_{ij}-\dot{\varepsilon}_{ii}/3$ denotes deviatoric strain rates, G the elastic shear module, $\dot{\lambda}$ the plastic multiplier, Q the plastic flow potential (defined below), σ_{ij} stress, and D/Dt denotes the objective derivative of the stress tensor (Hutter and Jöhnk, 2004)

$$\frac{D\tau_{ij}}{Dt}=\frac{\partial \tau_{ij}}{\partial t}+v_j\frac{\partial \tau_{ij}}{\partial x_j}+\tau_{ij}W_{ij}-W_{ij}\tau_{ij}, \tag{5}$$

where $W_{ij}=(1/2)((\partial v_i/\partial x_j)-(\partial v_j/\partial x_i))$ is the vorticity. Viscosity, μ, is given by

$$\mu=\mu_0\left(\frac{\dot{\varepsilon}_{\mathrm{II}}}{\dot{\varepsilon}_0}\right)^{(1/n)-1}\exp\left[\frac{Q}{nR}\left(\frac{1}{T}-\frac{1}{T_0}\right)\right], \tag{6}$$

where $R=8.3145$ J/K/mol is the universal gas-constant, $\dot{\varepsilon}_{\mathrm{II}}=(0.5\dot{\varepsilon}_{ij}\dot{\varepsilon}_{ij})^{0.5}$ is the second invariant of the strain rate tensor, $\dot{\varepsilon}_0$ a characteristic strainrate, T temperature, T_0 a characteristic temperature, Q the activation energy, n the powerlaw exponent and μ_0 the effective viscosity at $T=T_0$ and $\dot{\varepsilon}_{ij}=\dot{\varepsilon}_0$.

Rocks cannot sustain high differential stresses; they will fail by some plastic mechanism instead. A large number of laboratory experiments indicate that under upper crustal conditions the strength of rocks increases with increasing confining pressure (Byerlee's law). At higher confining pressures, for example, under upper mantle conditions, the failure mechanism changes and becomes independent of depth. The exact plastic failure condition at these depths is more difficult to address in laboratory experiments. The few experiments that do exists, however, point to Peierls low-temperature plasticity as a strength limiting mechanism (Goetze and Evans, 1979; Regenauer-Lieb and Yuen, 2003). Finally, every material has a theoretical strength, which is the differential stress above which atom bonds break. This strength, called the Frenkel limit, is around one tenth of the elastic shear module ($\sim$ 10–100 GPa in rocks). Experimentally observed maximum strengths, however, are typically significantly smaller than this limit.

A frequently invoked, phenomological, law that describes much of the behavior mentioned above is Mohr–Coulomb plasticity. The yield condition, F, and plastic flow potential Q, for Mohr–Coulomb plasticity are given by

$$F=\tau^*-\sigma^*\sin(\phi)-c\cos(\phi), \tag{7}$$

$$Q=\tau^*-\sigma^*\sin(\psi), \tag{8}$$

where in 2-D, $\tau^*=\sqrt{((\sigma_{xx}-\sigma_{zz})/2)^2+\sigma_{xz}^2}$, $\sigma^*=-0.5(\sigma_{xx}+\sigma_{zz})$, c denotes cohesion, ϕ the friction angle, and ψ the dilatancy angle. In rocks, the dilatancy angle is typically much smaller than the friction angle ("non-associated plasticity"), which is why we assume $\psi=0$.

In addition to the mechanical system of equations described above, we should also solve the energy equation:

$$\rho c_{\mathrm{p}}\left(\frac{\partial T}{\partial t}+v_j\frac{\partial T}{\partial x_j}\right)=\frac{\partial}{\partial x_i}\left(k\frac{\partial T}{\partial x_i}\right)+H+H_{\mathrm{a}}+\tau_{ij}(\tilde{\dot{\varepsilon}}_{ij}-\tilde{\dot{\varepsilon}}_{ij}^{\mathrm{el}}), \tag{9}$$

where c_{p} is heat capacity, k thermal conductivity, H volumetric radioactive heat production, H_{a} adiabatic heat production, and the last term denotes shear heating due to non-recoverable processes.

We use the Boussinesq approximation and density is assumed to be a function of temperature:

$$\rho=\rho_0(1-\alpha(T-T_0)), \tag{10}$$

where ρ_0 is the density at some reference temperature T_0.

The mantle geotherm, in the absence of deformation, is adiabatic (Schubert et al., 2001). Consequently, only temperature differences with respect to the adiabat drive flow. Modeling such a system in a self-consistent manner requires either a fully compressible formulation, or an appropriate simplification such as the anelastic formulation (Tackley, 1996). Whereas the importance of adiabatic effects has been demonstrated for whole mantle flow (Tackley, 1996), they are likely to be a second order effect on the scale of the upper mantle. Therefore, we have ignored those effects in the simulations presented here. We do however take (elastic) compressibility into account in parts of the lithosphere. To be consistent with such a Boussinesq formulation for the mantle, we have therefore employed a constant (i.e. non-adiabatic) initial temperature structure in the upper mantle.

3. Numerical technique

3.1. Finite element formulation

The governing Eqs. (1)–(10) are solved with a finite element approach (SloMo) which employs a velocity–pressure formulation for the mechanical equations (Cuvelier et al., 1986; Hughes, 1987; Moresi et al., 2003), with quadratic elements for velocity and discontinuous linear shape functions for pressure. The energy equation (Eq. (9)) is solved with a separate finite element code employing quadratic elements. Time stepping is done in an implicit manner with an adaptive time step.

The code is employed in a Lagrangian manner, in which the elements are deformed at each time step. If the elements are too distorted, remeshing is applied, thereby maintaining topography. Stresses are stored at integration points, which has the advantage that stresses from the last time step satisfy the force balance equations. Upon remeshing, deviatoric stresses are interpolated from the old to the new grid using a nearest neighbor algorithm, which ensures that the incompressibility condition remains satisfied. After a remeshing step, a number (e.g. 50) of smaller time steps are taken to reestablish isostatic equilibrium.

3.2. Tracer-based material properties

Tracers are employed to track material properties as well as to record maximum temperatures, and pressures. Material properties are computed from tracers by computing the dominant phase at each integration point, after which the integration point values are averaged over the element.

Using tracers in combination with a Lagrangian FEM framework has the advantage that only local tracer coordinates are required (inside an element), since global coordinates can be retrieved by multiplying with the element shape function. Computing local coordinates is a relatively expensive operation; since it however should be done only upon remeshing, the tracer advection routine is an overall cheap operation (Poliakov and Podladchikov, 1992).

3.3. Surface processes

The finite element formulation employed here allows the use of a true free surface. In addition, we incorporate surface processes (erosion and sedimentation) by a 1-D diffusion equation

$$\frac{\partial h}{\partial t} = \frac{\partial}{\partial x}\left(k_{\mathrm{e}}\frac{\partial h}{\partial x}\right), \tag{11}$$

where h is the surface elevation and k_{e} a constant that is determined empirically (to give reasonable erosion rates).

3.4. Code verification

The accuracy of the numerical code has been verified by comparing results with available numerical and analytical solutions, including 0-D rheological tests (Kaus, 2005), comparison with analytical solutions of the 2-D and three-dimensional (3-D) viscous and viscoelastic Rayleigh–Taylor and folding instabilities (Kaus and Podladchikov, 2001; Kaus, 2005; Kaus and Schmalholz, 2006; Kaus and Becker, 2007), thermo-chemical convection (van Keken et al., 1997), free surface deformation (Poliakov and Podladchikov, 1992), thermal solutions (Turcotte and Schubert, 1982), shear localization (Kaus and Podladchikov, 2006) as well as with other numerical and analogue models of brittle, upper crustal, deformation (Buiter et al., 2006).

4. Model setup

4.1. Geological model inspiration

The purpose of this paper is to obtain insight in the dynamics of mountain-building processes at passive continental margins, which is likely to be relevant for the geodynamic evolution of Taiwan. Taiwan is located at the complex boundary between the Philippine Sea Plate (PSP) and the Eurasian (EUR) plate. Northeast of Taiwan, the PSP subducts underneath the EUR plate in the Northward direction. South of Taiwan, the oceanic part of the EUR plate actively subducts underneath the PSP in an eastward direction. This subduction reversal should be somehow accommodated underneath Taiwan, either by slab break off, slab tearing, or tearing of the Eurasian lithosphere. Most plate tectonic reconstructions indicate that before collision, the oceanic part of the EUR plate subducted underneath the overriding PSP plate, much like what happens currently south of Taiwan (Lallemand et al., 2001; Sibuet et al., 2002). Recent tomographic studies support this idea and indicate that a nearly vertical slab, connected to the EUR plate, is present underneath Taiwan (Wang et al., 2006).

Taiwan itself is a young orogeny that emerged from the sea roughly 5 million years ago, and has one of the highest erosion rates on Earth. Its mountains are mainly composed of mildly metamorphosed sediments that are derived from EUR passive continental margin and that have been rapidly exhumed, possibly after collision of the Luzon Arc in the PSP with the passive continental margin (Chai, 1972). The dynamics of mountain building processes in Taiwan has been subject of a long standing discussion, ever since Suppe proposed the critical wedge model for its formation (Suppe, 1981, 1984). The critical wedge model assumes that deformation is located in the upper crust only. This is inconsistent with seismological and geophysical data that provide evidence for involvement of the lower crust and upper mantle in the deformation of Taiwan (Wu et al., 1997). Subsequently, a number of alternative models have been developed which include a whole lithosphere collision model (Wu et al., 1997), slab detachment (Teng et al., 2000), crustal exhumation involving the lower crust (Lin and Watts, 2002), or accretion of continental crustal material following arc-continent collision (Malavieille et al., 2002; Chemenda et al., 1997).

Clearly, a detailed understanding of the geodynamic processes that formed Taiwan requires fully three-dimensional simulations that are capable of computing mantle, lithosphere and surface processes in a self-consistent manner. Whereas such models are slowly emerging, they remain computationally expensive. Moreover the dynamics of the lithosphere is incompletely understood even in 2-D. Here we therefore focus on simplified, two-dimensional, numerical experiments, which broadly mimic the pre-collisional geometry of the Taiwan region.

4.2. Initial geometry and rheologies

Our model setup consists of an oceanic plate subducting underneath the overriding PSP (Fig. 1). The PSP consists of a 10 km thick crust and an oceanic mantle–lithosphere, whereas the continental part also includes a passive continental margin at the

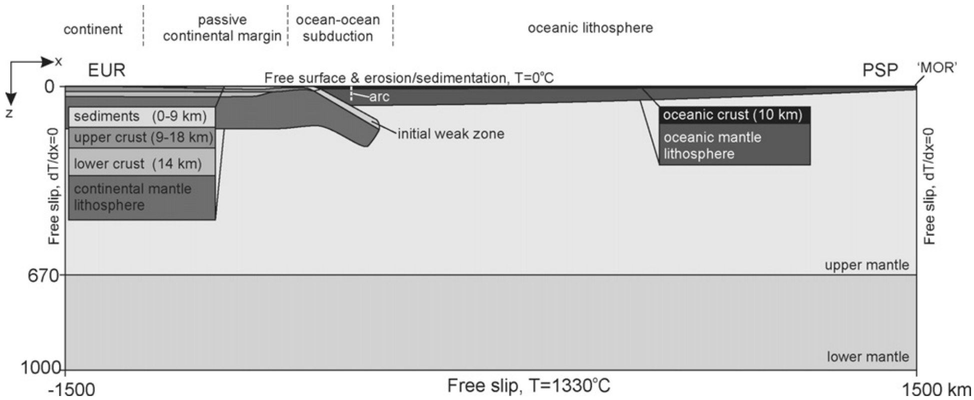

Fig. 1. Numerical model setup (see text for more details). Grid resolution 361 × 121 nodes with mesh refinement around the trench area. In some simulations, an oceanic arc was included in the overriding plate.

transition between the subducting part and the stable EUR continent. The lithosphere and mantle are composed of different phases, each with its own material properties. The following phase transitions are incorporated: (1) the 670 km transition (resulting in a 30-fold viscosity increase for mantle materials), (2) the mantle–lithosphere/asthenosphere transition at 1250 °C (below this, asthenosphere transforms into mantle–lithosphere and vice versa), (3) sediments transform into a weak zone (10^{20} Pa s), once they are subducted below a depth of 30 km and have a temperature larger than 450 °C.

Temperature-dependent densities are considered in all cases. In all but a few cases rheology is visco-elasto-plastic. Even though elastic and plastic effects are taken into account, they are only important in near-surface areas since the Maxwell relaxation times and stresses in, for example, the mantle are sufficiently small to make them behave in an effectively viscous manner.

For reasons of simplification, we have restricted our analysis to linear, material-dependent, viscosities. We are aware that laboratory experiments suggests that rocks, in most cases, have non-linear temperature-dependent effective viscosities (Ranalli, 1995). Incorporating such viscosity laws into numerical models however dramatically increases the (already significant) number of parameters. Moreover, several measured parameters of laboratory creep laws are still uncertain, and potentially important variations in crustal composition or volatile concentrations unknown (Ranalli, 2003; Burov, 2003). We therefore use constant, material-dependent Newtonian flow with viscosities which we deem appropriate for an effective rheological description of the major components of the crust and mantle within the model domain. While less realistic than nature, this simplification has the benefit that the fundamental dynamics of the system can be easier understood.

All models shown here employed the setup illustrated in Fig. 1. In models with a younger thermal age of the continent, the mantle–lithosphere was thinner (since the mantle–lithosphere was taken to be a function of temperature). Moreover, in a few cases we have inserted an oceanic arc in the overriding PSP plate, about 100 km away from the subduction zone. This was done by either increasing the temperature (linearly over a zone of 100 km with minimum age 27 Myrs) and crustal thickness (to 20 km thickness over a 50 km wide zone) or by decreasing the viscosity throughout the lithosphere. The subducting plate has an initial angle of 30° and has a 25 km thick weak zone on top.

In some models, we simulated the effect of slab break-off. This was done by 'cutting-off' the slab after a certain time (e.g. 10 Myrs), through changing slab material into mantle material.

4.3. Initial thermal structure

The initial temperature structure of the simulations is computed from 1-D models in which a constant temperature material is cooled for a given amount of time (the 'thermal age'), taking into account layers with radioactive heat production. In the oceanic lithosphere, the geotherm is age-dependent and increases linearly from 0 Myrs (at the 'mid-oceanic ridge') to 30 Myrs (close to the subduction zone). The continental lithosphere and the subducting slab have fixed ages, varying from 20 to 100 Myrs.

In a number of simulations we studied the effects of an oceanic arc in the overriding oceanic plate. In these simulations an arc was represented by either a thickened crustal layer and younger thermal age, or by adding a lithospheric-cutting, 20 km wide, weak zone in the mantle–lithosphere. Shear-heating was considered in all simulations.

4.4. Boundary conditions and numerical parameters

We assume insulating thermal boundary conditions at the sides of the box and isothermal conditions at the bottom and top. The gradient in thermal thickness of the oceanic lithospheric causes topography and ridge push, driving the oceanic plate toward the subduction zone. In addition, the initial subducting oceanic lithosphere drives flow due to its buoyancy. Lateral model boundaries are free slip and insulating. The lower boundary is free slip and has a constant temperature of 1330 °C.

The effect of surface processes is modeled by a diffusion-type equation (Eq. (11)). Since erosion is more efficient above than below the sea level (Simpson, 2006), we use $k_e = 0$ for elevation more than 1000 m below the average continental elevation (at the left side of the model). Employed values of k_e varied from 1000 m^2 yr^{-1} (resulting in average erosion rates of 1–2 mm/yr) to 10, 000 m^2 yr^{-1} (3–4 mm/yr).

In a number of simulations, we have studied the effects of boundary conditions on lithospheric-scale evolution. In these simulations, the upper boundary was taken to be a free surface. We also tested the effects of simplifying the rheology on model evolution, by deactivating plastic or elasto-plastic rheologies.

The grid resolution was 361 × 121 nodes, with grid refinement around the trench area, which resulted in nodal spacing that varied from ∼ 14 to 2.5 km. Around 300, 000 tracers have been employed, with a greatly increased tracer density near the trench. Time steps were adaptive and variable, but never larger than ∼ 10, 000 years, which was required for stability reasons due to the presence of the deforming free surface. Models have been initiated from a flat

Table 1
Standard model parameters

Material	Thickness (km)	ρ_0 (kg m^{-3})	μ_0 (Pa s)	K (Pa)	c (MPa)	$\phi(^\circ)$	H (W/m^3)
Lower mantle	330	3300	3×10^{21}	∞	–	–	0
Upper mantle	$\sim$ 520–650	3300	10^{20}	∞	–	–	0
Continental mantle–lithosphere	temperature dependent	3300	10^{22}	5×10^{10}	1000	0	0
Weak zone	20	3300	10^{20}	5×10^{10}	20	5	0
Upper continental crust	9–18	2750	10^{22}	5×10^{10}	20	30	10^{-6}
Lower continental crust	14	2750	10^{20}	5×10^{10}	20	30	10^{-6}
Sediments	0–9	2750	10^{20}	5×10^{10}	20	30	10^{-6}
Oceanic crust	10	2950	10^{23}	5×10^{10}	20	30	0
Oceanic mantle–lithosphere	temperature dependent	3300	10^{23}	5×10^{10}	1000	0	0

$\alpha = 3 \times 10^{-5}$ K^{-1}, $G = 5 \times 10^{10}$ Pa, $k = 3$ W/m/K, $c_p = 1000$ J/kg/K for all phases. The thermal age of the continental side is 65 Myrs, and that of the overriding oceanic plate varies linearly from 0 to 30 Myrs. Erosional diffusivity was taken to be $k_e = 1000$ m^2 yr^{-1}.

topography, which resulted in a primary phase of isostatic adjustment (lasting $\sim 10,000$–$100,000$ years depending on employed viscosity and density variations). After this (not counted as time in the simulations), regular model evolution started.

5. Results

Model parameters employed in the standard run are summarized in Table 1. In the initial stages of the model, deformation is dominated by both ridge push and slab pull (Fig. 2). No external forcing is imposed. During these stages, the continent deforms in a relatively homogeneous manner and the passive continental margin moves toward the subduction zone. Once continental material arrives at the trench, the subduction zone steepens and becomes nearly vertical. After the steepening stage, the continental crust deforms in a vertically non-coherent manner with significant flow in the lower crust and more rigid deformation in the upper crust. This results in a relatively rapid exhumation of sediments and upper crust in a dome-like structure. Whereas the lower part of the oceanic mantle–lithosphere is incorporated in the subduction process, the upper parts and the oceanic crust are only slightly deformed. Control runs (not shown), in which the continent was not present, resulted in slightly shallower subduction angles. Most simulations result in a somewhat symmetric, “ablative” style of subduction in which the oceanic plate enters the trench from the right, consistent with previous analogue and numerical models (Tao and O’Connell, 1992, 1993).

5.1. Effect of lithospheric density structure

The effect of changing the lithospheric density structure was studied by (1) varying the thermal age of continental lithosphere, and (2) by changing the density of the lower crust. The main effect of changing the density structure is to change the timescale of deformation (Fig. 3). The older the lithosphere, the higher its density, and the faster subduction and therefore crustal deformation occur. Note that simulations with slightly younger plates (e.g. 40 Myrs) evolve into similar structures after longer timescales.

Changing the density structure of the lower crust has a relatively small effect on mantle-scale subduction dynamics. On a crustal scale, it results in a slightly deeper Moho. It is noteworthy that the dome-like structure still occurs even if the density of the lower crust is significantly increased, such that it is significantly larger than the density of the overlying rocks. This indicates that the dome is related to compressional deformation, rather than to buoyancy-driven deformation.

The linear scaling of subduction speed with density contrast (via plate age) is expecting from Stokes sphere sinking (Turcotte and Schubert, 1982), and/or modified plate bending/subduction velocity analysis (Conrad and Hager, 1999).

5.2. Rheology of the lower crust

The effect of the rheological stratification of the passive continental margin was studied by performing simulations in which the viscosity of the lower crust was increased with respect to the standard model (Fig. 4). Results indicate that mantle deformation in all cases is very similar. Differences, however, can be observed on a crustal scale: if the viscosity of the lower crust is smaller than that of the upper continental crust (‘the weak lower crust case’), exhumation of the lower crust occurs. If, on the other hand, the lower crust has equal or larger viscosity than the upper crust (‘a critical wedge setup’), exhumation is confined to the upper crust and sediments. As will be shown later, this results in smaller exhumation and cooling rates.

5.3. Rheological stratification of the oceanic plate

The effect of rheology of the overriding oceanic plate is studied by varying either crustal viscosity, mantle viscosity or both (Fig. 5). The most important parameter is the viscosity of the oceanic mantle–lithosphere. Decreasing it yields significantly faster mantle flow, and as a result, more intense crustal deformation. The rheology of the oceanic crust, however, also plays a role: if it is decreased w.r.t. the standard model the crust thickens significantly (which is probably unrealistic). If it is increased, on the other hand, comparatively little differences can be observed.

If both oceanic and continental mantle–lithosphere have a smaller and equal viscosity of 3×10^{21} Pa s, and the ocean crust is sufficiently strong (10^{24} Pa s), the oceanic crust separates from the mantle–lithosphere and overrides the passive continental margin (Steedman, 2007).

5.4. Effects of surface processes

The effect of surface processes was studied by increasing the erosional diffusivity k_e. Results show that erosion, for the present setup, does not have a significant influence on mantle flow (Fig. 6). Crustal evolution, however, is distinctly different and clearly influenced by erosion. If erosion is absent, little deformation occurs in the crust. If erosion rates are large, crustal structures become close to vertical and deeper crustal levels are exhumed.

If erosion is activated in the presence of a strong lower crust, such an exhumation is not observed (Steedman, 2007). Instead, the models evolve very similar to the strong lower crust cases of Fig. 4, with little exhumation of deep crustal levels.

Erosion rates are not constant throughout the model evolution. Typically, erosion rates are small in the beginning (when topography is small), and increase after ~ 5 Myrs model evolution. Erosion rates after 30 Myrs model evolution vary from 1–2 mm/yr (for

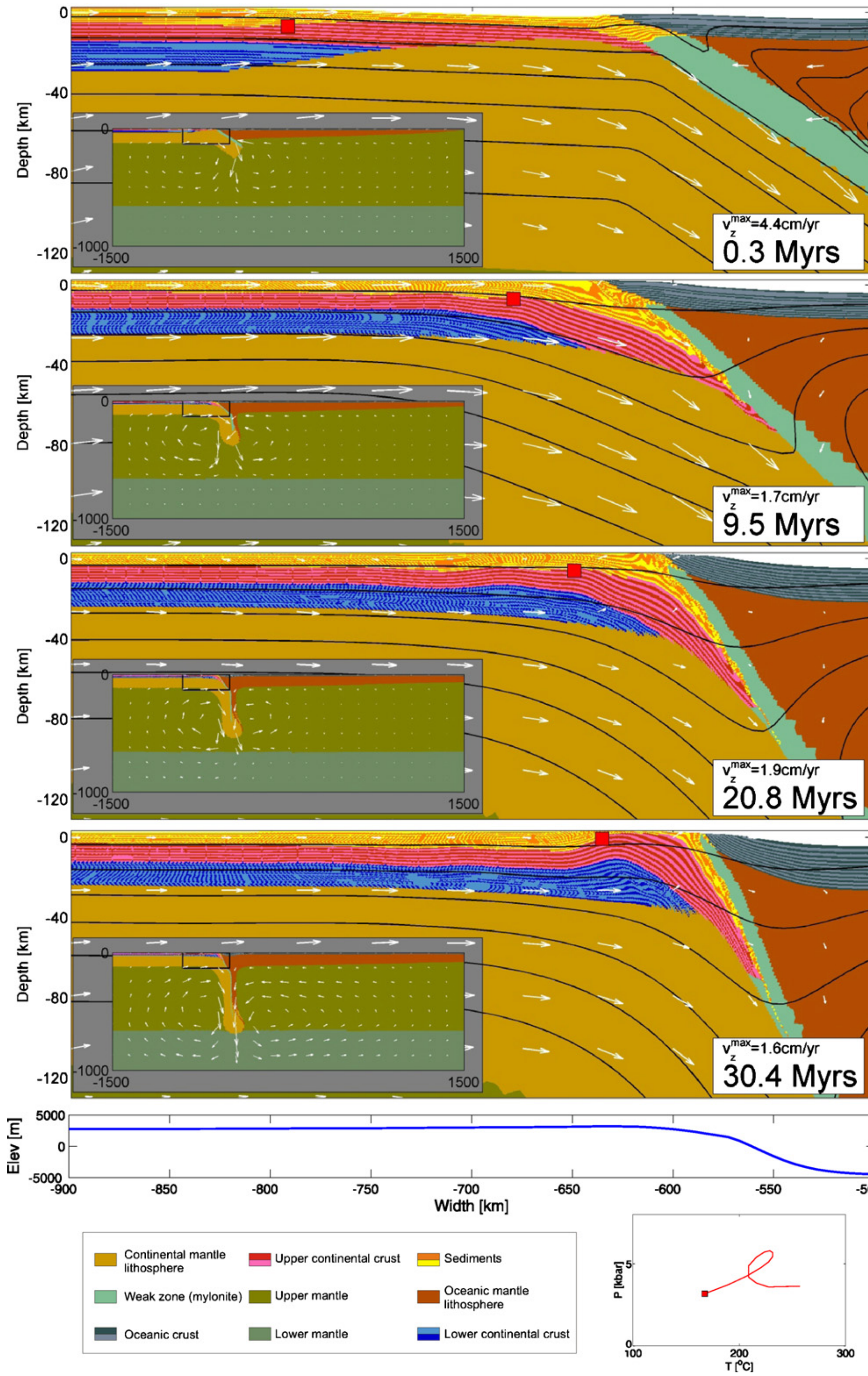

Fig. 2. Time evolution of the standard model showing the phase distribution (upper panels), topography at 30 Myrs and *P*–*T* evolution of a tracer in the upper crust. Temperature iso-contours are displayed every 100 °C. The maximum vertical velocity, v_z^{max}, in the whole domain is indicated. The subduction results in strong crustal deformation once buoyant continental material enters the subduction zone (after ~ 10 Myrs). Model parameters are specified in Table 1.

$k_e = 1000\,m^2\,yr^{-1}$) to 3–4 mm/yr (for $k_e = 10,000\,m^2\,yr^{-1}$). Note that due to the use of a diffusion-type erosion equation, these rates represent orogen-averaged rates and can therefore not be directly compared to local erosion rates (which may be significantly larger).

5.5. Effects of boundary conditions

In typical mantle convection models, the surface of the Earth is approximated with a free-slip boundary condition (in some cases coupled to an evolving dynamic topography). Many lithospheric-

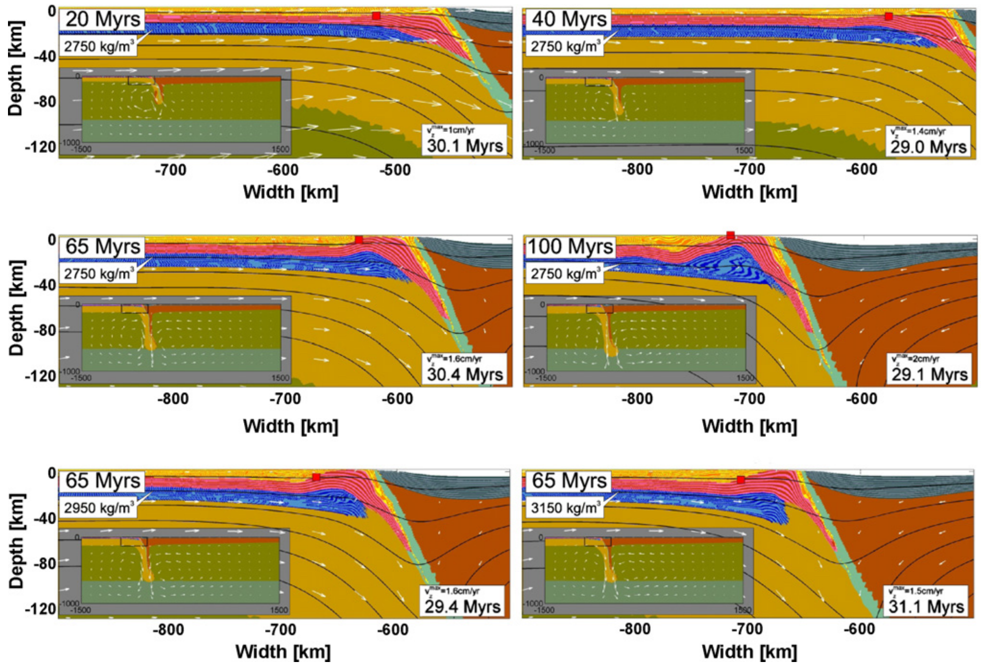

Fig. 3. Effect of changing the thermal age of the continent (upper 2 rows) and the density of the lower crust (lowermost row). Colors as in Fig. 2. Note different *x*-axes in the 20 Myrs case.

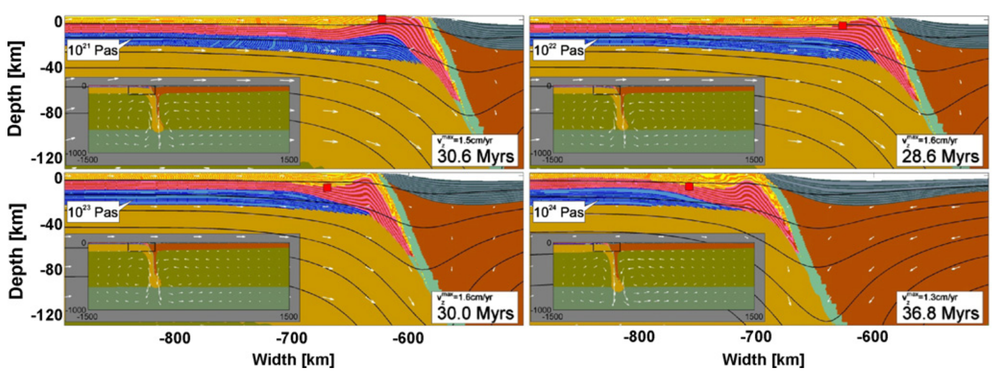

Fig. 4. Effect of lower continental crust viscosity, while keeping other model parameters constant. Mantle deformation is similar in all cases. Crustal deformation differs, depending on whether the viscosity of the lower crust is smaller or larger than the viscosity of the upper crust (10^{22} Pa s). Legend as in Fig. 2.

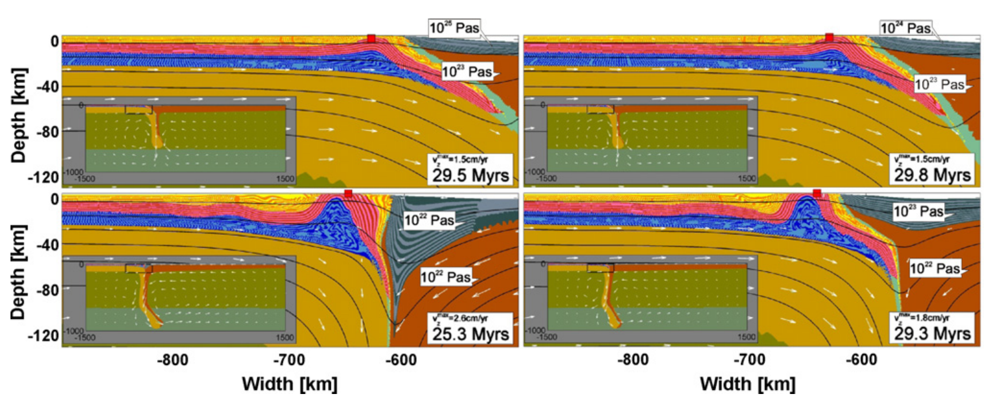

Fig. 5. Effect of oceanic crust and mantle–lithosphere viscosity on model evolution. If the viscosity of the oceanic crust is increased with respect to the standard model (10^{23} Pa s), more continental material is subducted (upper two panels). If it is decreased, significant thickening of the lower crust occurs (lower left). If the viscosity of the oceanic mantle–lithosphere is lower than the standard case (with 10^{23} Pa s), subduction occurs significantly faster and results in more crustal exhumation (lower two panels). Colors as in Fig. 2.

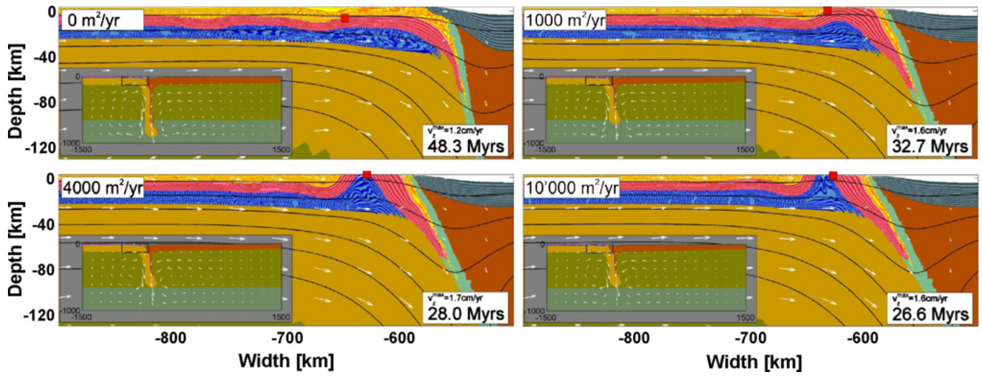

Fig. 6. Effect of surface processes (expressed through the erosional diffusivity k_e) on model evolution. Increasing the erosion rate enhances the lower crustal bulge, but has little effect on mantle-scale deformation.

deformation codes, on the other hand, explicitly incorporate and track the free surface. Since numerical simulations with a deforming free surface are numerically more demanding than free slip simulations (due to significant time-step restrictions), it is interesting to understand the effects of the upper boundary condition on model evolution. Fig. 7 compares the standard model with that of a model in which the upper boundary was taken as free-slip. The flow at depth is nearly identical in both cases. The crustal evolution, however, does show differences. A comparison with the erosion-absent simulation of Fig. 6 illustrates that most of these differences are caused by the effects of erosion.

It thus seems that, for the present setup, erosion and the surface boundary condition have a minor effect on mantle flow and it is in this case safe to approximate the surface with a free-slip condition. If, on the other hand, one is interested in crustal-scale processes, erosion can play a significant role and the surface should be approximated by a free surface.

5.6. Presence of an arc

In Taiwan, much of the mountain belt evolution is thought to be due to the collision of the Luzon Arc with the passive continental margin (Lallemand et al., 2001). Whereas arc-related rocks are indeed present in Eastern Taiwan, it is not clear whether all of the exhumation can be attributed to arc-continent collision (Lee et al., 2006). In order to study the effects of an oceanic arc on model evolution we have performed a set of runs in which an oceanic arc was emplaced in the overriding PSP plate. The arc was represented by (1) either a zone of thickened oceanic crust and smaller thermal age, or by (2) weakening the mantle–lithosphere over its whole thickness though a 20 km wide weak zone.

Results (Fig. 8) are identical to the standard case if the thermal arc is initially sufficiently far away (e.g. 300 km). If the thermal arc is closer to the initial subduction zone, it results in faster rates of subduction and a slightly more intense crustal deformation. If,

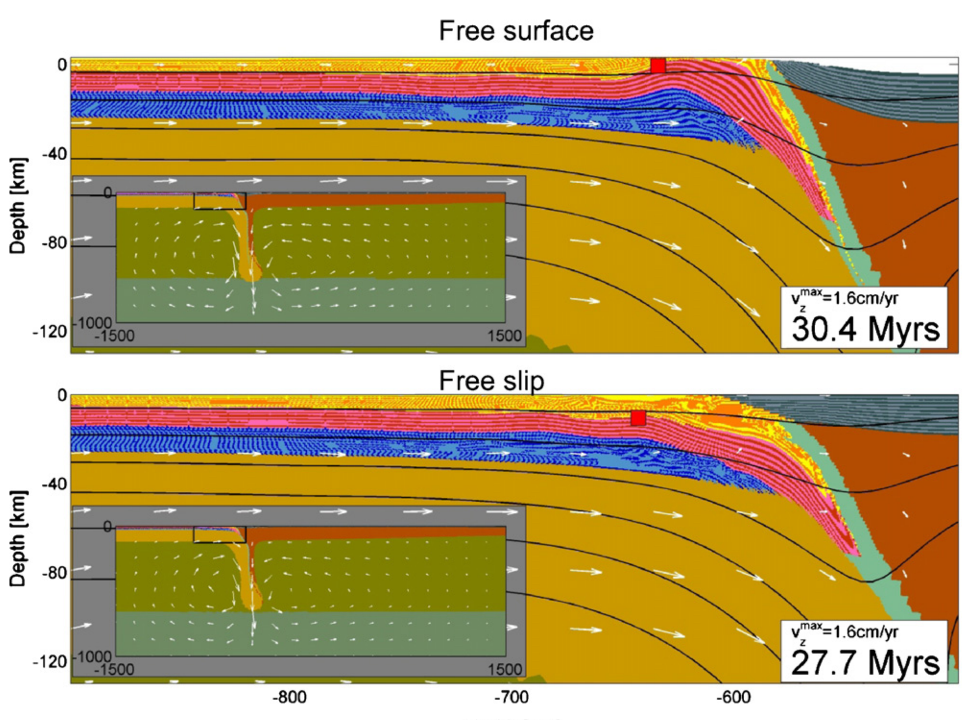

Fig. 7. Effect of surface boundary condition on model evolution.

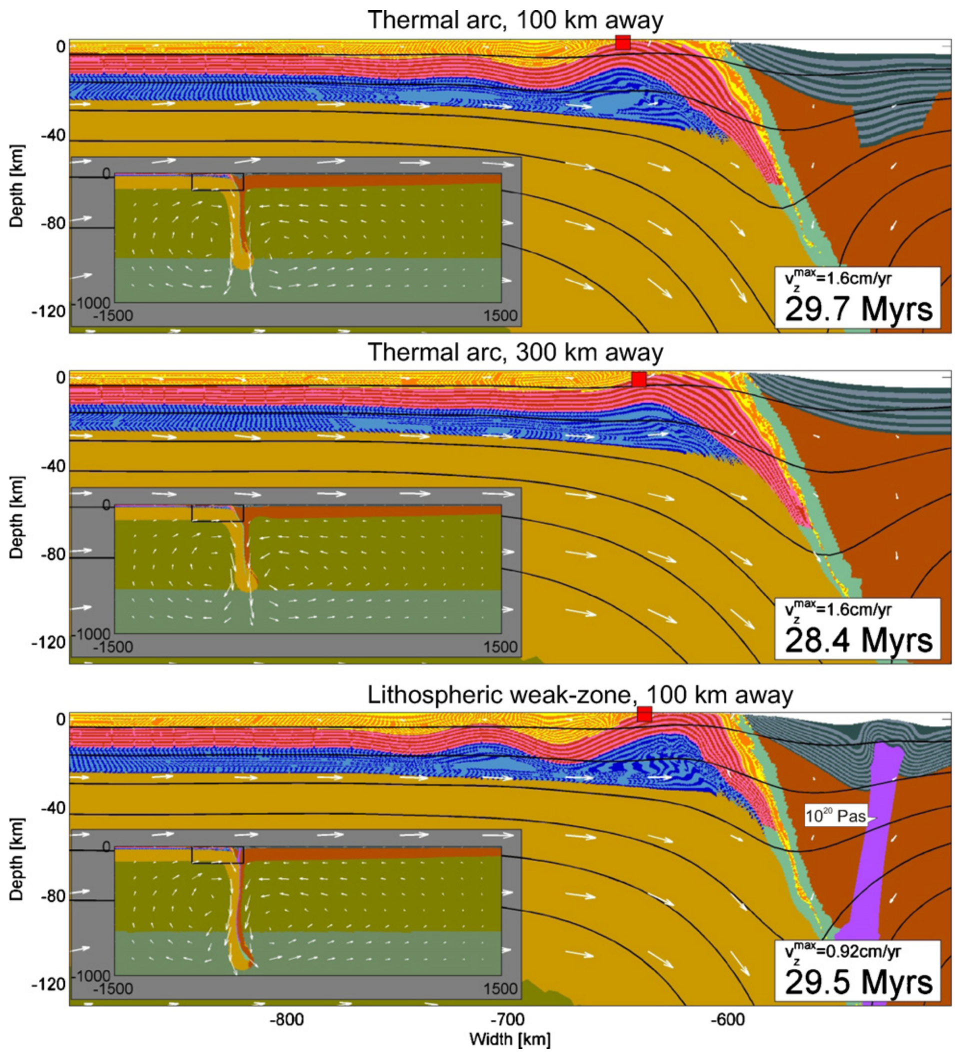

Fig. 8. Effect of an arc in the overriding oceanic plate. The arc has been implemented as either a thickened crust and thermally enhanced zone (upper two panels) or as a lithospheric-cutting vertical weak zone (lower panel).

on the other hand, the arc is a zone of significant weakness (as was assumed in e.g. the laboratory experiments of Chemenda et al. (2001)) subduction evolves significantly faster, which in turn has a profound effect on crustal evolution (Fig. 8).

5.7. Viscoelastoplastic versus viscoelastic and viscous rheology

Many mantle convection and lithospheric deformation models represent the mantle as having a viscous or a viscoplastic rheology. Others, including the one here, include a more complex visco-elasto-plastic rheology. Whereas such a rheology is clearly more realistic, it is at this stage not clear to which extend this complexity changes model results. For this reason we have repeated the standard model with simulations in which plastic and elastoplastic deformation mechanisms have been deactivated. Results (Fig. 9) are very similar in all cases, indicating that viscous deformation is the dominant mechanism in most models presented here. This is not entirely surprising since most of the large scale flow in our models is caused by density-driven sinking of the mantle–lithosphere. Kaus and Becker (2007) analyzed the effect of elasticity on density-driven flows and found it to be significant only if the Deborah number, defined by $De = (\Delta\rho g H/G)$, is larger than 0.1–1 (here $\Delta\rho$ is a characteristic density difference, H a characteristic length scale, g gravitational acceleration, and G the elastic shear module). In the present setup, $De \sim 0.01$, and hence elasticity is predicted to play a minor role on the subduction dynamics.

Of course, one should be careful in generalizing these observations, in particular since previous workers have demonstrate the importance of elasticity or plasticity on certain lithospheric-scale instabilities such as buckling (Schmalholz and Podladchikov, 1999; Schmalholz et al., 2002) or the onset of shear-localization (Kaus and Podladchikov, 2006; Regenauer-Lieb and Yuen, 2003).

5.8. Mantle–lithosphere coupling

To obtain insight in the control of crustal-scale processes on mantle processes, we have computed slab depth and trench-location through time for several of the end-member models. As trench location we used the left-most boundary between oceanic crust and sediments or upper crust.

Results (Fig. 10) quantify that models with significantly different crustal evolution, such as the free-slip or the fast erosion model, can have identical mantle deformation. Thus, in these cases, mantle deformation is clearly decoupled from crustal deformation.

The main factors that affect the rate of subduction are coupling of the subducting with the overriding plate and the density

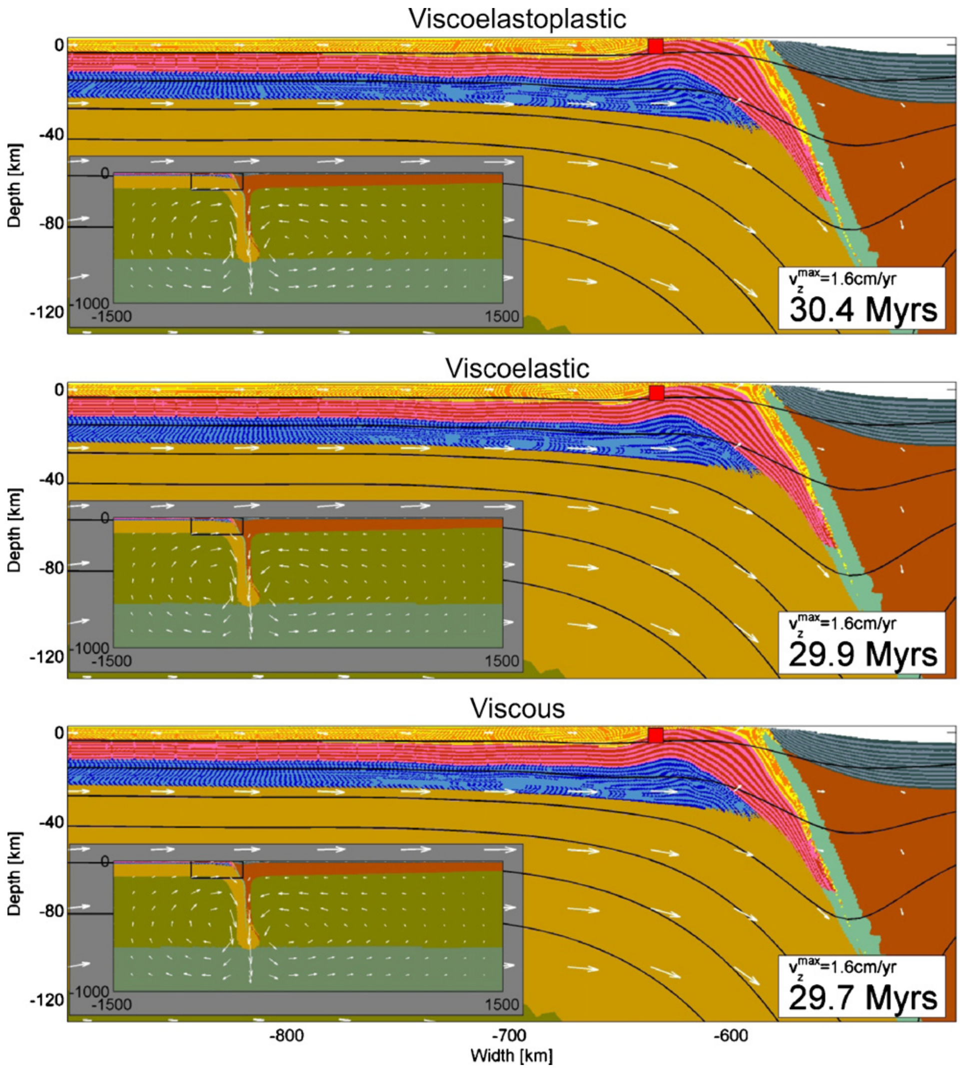

Fig. 9. Comparison of simulations with a viscoelastoplastic rheology, a viscoelastic rheology and a viscous rheology. Model evolution is similar in all cases.

structure of the subducting plate. If coupling is weak, for example, because a weak arc (Fig. 8) is present, the subduction rate significantly increases. If the available buoyancy is smaller, for example, because the plate is younger, the subduction rate is smaller.

The subduction rate is not directly linked to the rate of trench migration. In most simulations, the trench remains more or less stationary, whereas a younger continent results in trench advancement. Interestingly, a strong lower crust has a profound effect on trench migration (Fig. 10B) whereas it has a negligible effect on the subduction velocity (Fig. 10A). Visual inspection of the simulation shows that this is caused by a more asymmetric crustal deformation.

5.9. Metamorphic facies, cooling rates and thermo-chronological data

To allow comparison of model results with observed metamorphic facies we have computed the maximum temperature (and accompanying pressure) for each of the tracers in the models and compared those values with a metamorphic facies map (Winter, 2000). The results, presented as synthetic metamorphic cross-sections, show that most of the surface-near rocks are expected to be in the zeolite facies (Fig. 11). If fast erosion and a weak lower crust are present, however, both prehnite-pumpelyite and greenschist facies rocks are exhumed to the surface, in agreement with observations in Taiwan (Lee et al., 2006).

It should be noted that the boundaries between different facies are somewhat diffuse and dependent on rock chemistry (Spear, 1994). Moreover, not all metamorphic facies are expected to occur in reality since the rate of metamorphic reactions is sensitive to reaction kinetics, which is in particular controlled by the presence of water. Cross-sections computed on the basis of other facies maps are thus slightly different in detail. The overall characteristics, however, appear robust and can thus be compared with observations.

A different type of dataset that recently became available for Taiwan is thermo-chronology, which records the closure-age of various mineral systems (Willett et al., 2003; Lee et al., 2006) and, from this, the cooling rates of rocks currently exposed at the surface. We have computed cooling-rates from our models by computing the averaged temperature difference $\Delta T/\Delta t$ for each tracer over the last ~ 1 Myrs. The results clearly illustrate the effect of erosion and lower crustal flow on cooling rates (Fig. 11). Whereas average cooling rates are on the order of ~ 10 to $\sim 20\,^{\circ}$C/Myrs, rates of up to $\sim 70\,^{\circ}$C/Myrs are obtained if erosion rates are sufficiently high.

A further way of representing the data is shown on Fig. 12. Here, the temperature of a number of tracers is plotted versus time, together with observations from fission track data (Lee et al., 2006).

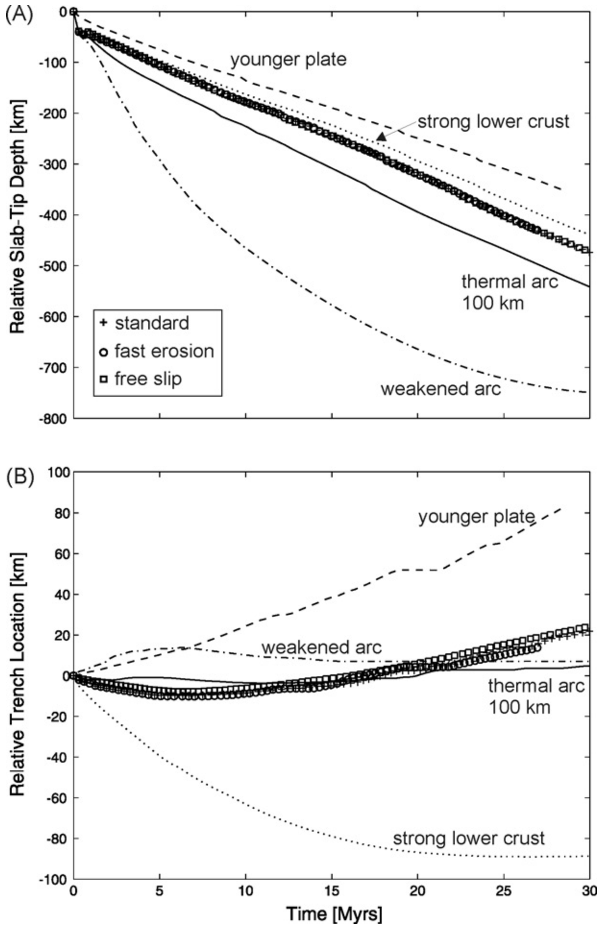

Fig. 10. (A) Maximum slab depth versus time. (B) Trench location versus time, both with respect to starting location. The following parameters have been employed: fast erosion model— $k_e = 10,000\,\mathrm{m^2\,yr^{-1}}$; strong lower crust— $\mu_{lc} = 10^{24}$ Pa s; younger plate—20 Myrs. Other parameters as specified in text.

The tracers were taken in the center of the model, above the location of highest cooling rate. Models are compared with data from Southern Taiwan, because here the Luzon Arc did not collide yet with the mainland of Taiwan, which more closely resembles our model setup. Lee et al. (2006) demonstrated that in Southern Taiwan, an age-progression occurs between the southern-most tip of Taiwan (with smaller cooling rates) toward the north (with highest cooling rates). Comparison with model results shows that there is a remarkable agreement if a weak lower crust and efficient erosion are present. Models that do not have these features have smaller exhumation rates, and consequently, lower grade metamorphic facies exposed at the surface.

In Northern Taiwan, where the Luzon Arc collision with the Taiwanese mainland already occurred, both peak metamorphism and cooling rates are larger than in Southern Taiwan (Lee et al., 2006). It seems likely that this effect can be reproduced with our models if tuned accordingly (the weak arc simulation, for example, does result in somewhat larger exhumation rates).

Models in which erosion rates are smaller, or the lower crust is stronger coupled to the subducting mantle–lithosphere, result in smaller exhumation rates. The basic assumption of many kinematic modelling approaches, however, is that a strong coupling between mantle and crust exists. Such models thus might need refinement if applied to cases in which the lithospheric rheology is strongly layered in the vertical direction.

6. Insight in the physics of crustal exhumation from simplified numerical and analytical models

The numerical models presented so far indicate that the rheology of the lower crust and the erosion rate are the two key parameters that control the exhumation rate in small scale mountain belts in the setup employed here. Whereas this is an interesting observation, it sheds little light on the underling physics of the geodynamic processes. Moreover, even though our numerical models are simplified in many aspects, they still have at least 35 parameters (not counting initial model geometry—see Table 1). If we were to perform systematic numerical experiments in a brute force manner, and we would use two values for each of the parameters, a total of $2^{35} \approx 3 \times 10^{10}$ simulations are required to cover the parameter space. Given that each simulation takes a couple of days, such an approach is clearly unfeasible. Instead, most workers use their experience in choosing the key parameters that are varied in the setup. Here we use an additional approach in which we extract a simplified model-setup from the full geodynamic simulations and study this setup with (semi-)analytical approaches and numerical models.

From many of the models, it seems that the subduction of the EUR oceanic plate together with the movement of the overriding PSP plate causes a state of compression in the continental crust (Fig. 13 A). This crust can broadly be regarded as a two-layer system consisting of a brittle upper crust and a ductile lower crust subjected to uniform compression with background strainrate $\dot{\varepsilon}_b$ (Fig. 13B). Moreover, gravity is present, the upper surface is free and subjected to erosion and deposition (through Eq. (11)) and the lower boundary is a no-slip boundary. From the lithospheric-scale numerical models we infer that the background strainrate, $\dot{\varepsilon}_b =\sim 10^{-15}$ $\mathrm{s^{-1}}$.

Analytically, this setup is tractable if the rheology is considered to be powerlaw viscous, with viscosity defined as $\mu = \mu_0 \dot{\varepsilon}_b^{(1/n)-1}$. The brittle upper crust is approximated by a depth-dependent, powerlaw viscosity and computed such that differential stresses due to the compressional background deformation, are equal to the Mohr–Coulomb yield stress (Eq. (7)). Given these approximations, we can employ a standard perturbation technique to solve the governing equations and growth rate (Smith, 1977; Fletcher and Hallet, 1983; Zuber, 1987; Bassi and Bonnin, 1988; Montesi and Zuber, 2003), for a single sinusoidal perturbation which is looped over all possible wavelengths down to the minimum resolvable lengthscale. Since viscosity has a linear depth-dependency, a closed form analytical solution is difficult to derive. Instead, we employ a multi-layer approach in which the depth-dependent brittle crust is approximated by discrete linear layers (Bassi and Bonnin, 1988; Montesi and Zuber, 2003). The semi-analytical approach yields vertical velocities for each of the layer interfaces, which are in turn used to integrate interface amplitude forward in time (employing implicit time discretization as described in Kaus and Becker (2007)). Surface erosion and redeposition is employed at the surface at every time-step, and an averaged, exponential, growth rate is computed for the upper crust/lower crust interface once a finite amplitude (3 km) is reached from initially small (100 m) perturbations. Much like in the classical folding instability a single wavelength exists for which the growth rate has a maximum q_{dom}.

A contour plot of the normalized dominant growth rate as a function of erosion rate and viscosity of the lower crust reveals that different domains exists in which the iso-contours of $q_{\mathrm{dom}}/\dot{\varepsilon}_b$ have different orientation (Fig. 13C). This indicates that different physical mechanisms are active in each of the domains. The fast-erosion domain, for example, is insensitive to further increases in erosion rate, indicating that topographic stresses are small compared to flow-induced stresses. The gravity-controlled domain, on the other

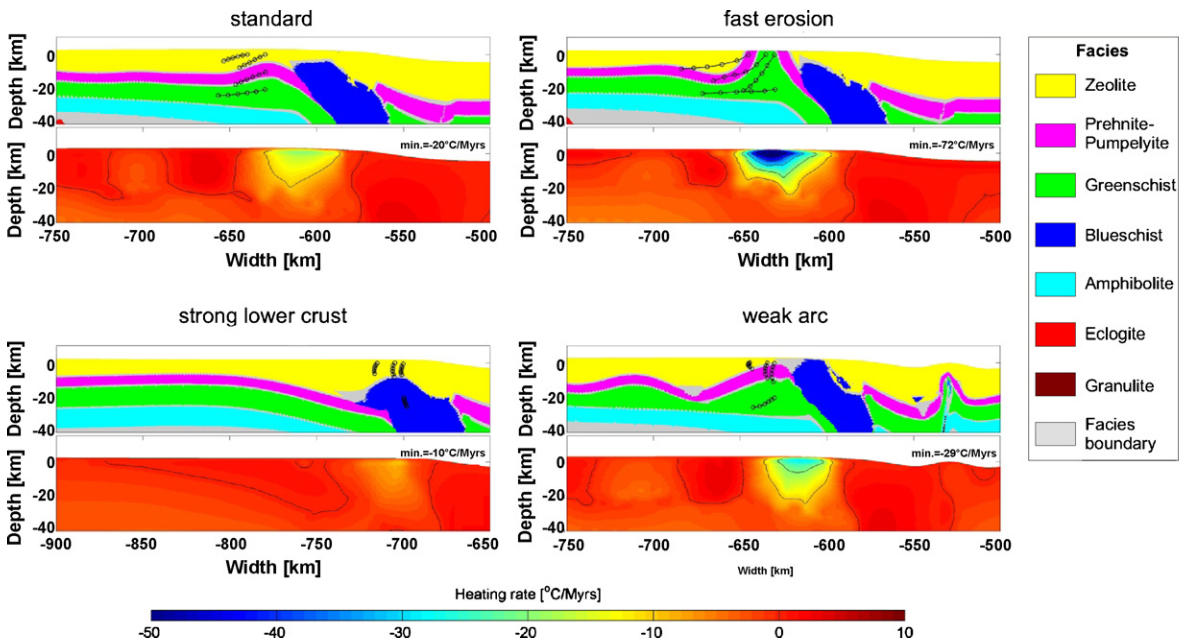

Fig. 11. Metamorphic facies and heating rates for a zoomed-in part of the crust for four end member models. Also plotted are particle paths for the last 10 Myrs (black lines with circles every 2 Myrs). Heating rates are an average of the last ~ 1 Myrs. Highest cooling rates occur if erosion is efficient and the lower crust is weak, which is accompanied by exhumation of greenschist facies rocks to the surface. If, on the other hand, erosion rates are smaller or the lower crust is stronger ("critical wedge model"), exhumation rates are significantly smaller. Note that we take into account that boundaries between various metamorphic facies are somewhat diffuse (gray areas).

hand, exists if erosion rate is negligible and has small $q_{\text{dom}}/\dot{\varepsilon}_{\text{b}}$-values. Here, topographic stresses decrease the growth rate of the instability. As a rule-of-thumb, folding theory showed that $q_{\text{dom}}/\dot{\varepsilon}_{\text{b}}$ should be larger than 10–20 to obtain visible structures, as smaller values result in a pure-shear thickening mode of the crust. If both the upper and the lower crust are linearly viscous, such growth rates are obtained for $k_{\text{e}} > 1000\,\text{m}^2\,\text{yr}^{-1}$ and $\mu_{\text{LC}} < 5\times10^{20}$ Pa s (Fig. 13C).

The analytical theory provides useful insights (further outlined below). It however makes a number of simplifying assumptions

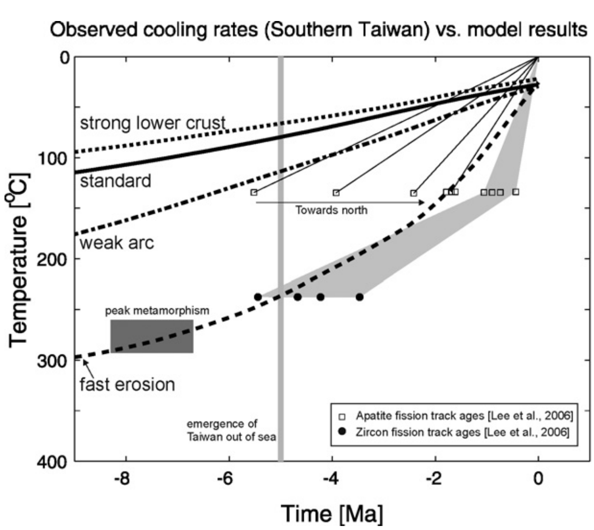

Fig. 12. Observed versus modelled thermo-chronological data. Observations are from Southern Taiwan, based on zircone and apatite fission track ages (Lee et al., 2006). Modelled data is computed from near-surface tracers above the highest cooling-rate areas of the numerical models displayed Fig. 11. The combination of weak lower crust and efficient erosion yields results that are in reasonable agreement with observations. Note that apatite ages indicate increasing cooling rates from Southern Taiwan toward North.

that may limit its applicability to the real, finite amplitude, world. It is therefore useful to cross-verify analytical results with numerical simulations. Here, we use SloMo to perform systematic calculations for the setup of Fig. 13B, with the difference that the upper crust was approximated by a visco-elasto-plastic layer, with shear module $G = 5.10^{10}$ Pa, viscosity $\mu = 10^{23}$ Pa s, cohesion $c = 40$ MPa and friction angle 30°. Simulations were initiated from an initially horizontal interface between upper and lower crust, which has been perturbed with random noise of maximum amplitude 500 m. Simulations have been performed for maximum 2.5 million years, after which the maximum deflection of the lower/upper crust interface, $\Delta A = \max(H) - \min(H)$, was compared to the total amount of thickening of the crust caused by background deformation, ΔH_c. The non-dimensional number $D_{\text{o}} = \Delta A/\Delta H_c$ was than used to distinguish fully developed domes ($D_{\text{o}} > 1$) from starting ($0.1 \le D_{\text{o}} \le 1$) and failed ($0.1 < D_{\text{o}}$) domes. Comparison of the numerical results with the analytical theory shows a remarkable agreement between the two approaches (Fig. 13C), if the brittle layer is linearly viscous. Reasonable agreement also exists between numerically and analytically computed dominant wavelength over thickness ratios, although numerical values are typically slightly smaller. It should be noted that numerically computed dominant wavelengths require very large aspect-ratio boxes. Moreover, uncertainty in determining dominant wavelengths stems from the tendency of, in particular, erosion-controlled modes to result in strong localization of deformation. Once the first dome has gained significant amplitudes, it changes the stress field and may prevent subsequent domes from developing a significant amplitudes. This phenomena is relatively well studied for single layer folding (Schmalholz and Podladchikov, 2000; Schmalholz et al., 2005; Schmalholz, 2006; Kaus and Schmalholz, 2006), and provides a possible explanation for the localized, rather than periodic, nature of the dome structures in our large-scale numerical simulations. It, however, makes it difficult to accurately determine dominant wavelengths from the numerical results.

If, in the analytical theory, the brittle layer is approximated by a layer with larger stress-exponent, the field of doming widens,

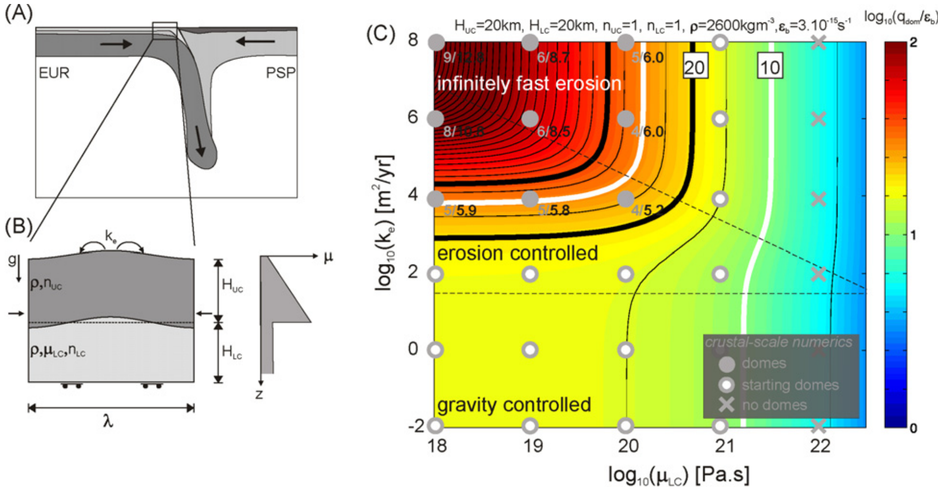

Fig. 13. (A) Cartoon illustrating the key observations of the lithosperic-scale models. Subduction of the oceanic part of the EUR plate, together with movement of the PSP plate results in a state of compression in the continental crust. (B) Setup for simplified analytical and numerical models. A two-layer system, consisting of a brittle upper and a ductile lower crust, is considered which is subjected to pure shear deformation and which is under the influence of gravity. The upper boundary is allowed to erode. In the analytical models, the brittle crust is treated as a powerlaw fluid with linear, depth-dependent, viscosity. In the crustal-scale numerical models, the brittle upper crust is treated as a frictional visco-elasto-plastic medium. (C) Analytically computed non-dimensional maximum growth rate as a function of lower crust viscosity μ_{LC} and erosional diffusivity k_e. Thin black lines are iso-contours (spacing 5). Symbols summarize the results of crustal-scale numerical computations. Numbers next to 'domes-mode' indicate numerically (gray) and analytically (black) computed dominant wavelength over thickness ratios. Reasonable agreement exists between analytics and the (simplified) numerics. The analytical results furthermore suggest that three doming modes exists, of which erosional-controlled modes are most efficient in crustal exhumation. Note that the analytical results are also in good agreement with the full lithospheric-scale numerical models of Figs. 4 and 6.

and fully developed domes are predicted to occur for lower rates of erosion, in apparent disagreement with our numerical results (Fig. 14). The reasons for this are not fully understood and will probably require the development of (new) analytical techniques capable of describing the evolution of multi-layered visco-elasto-plastic materials.

Whereas the details of the doming instability thus remain to be sorted out, we can employ existing theory to obtain insight in the

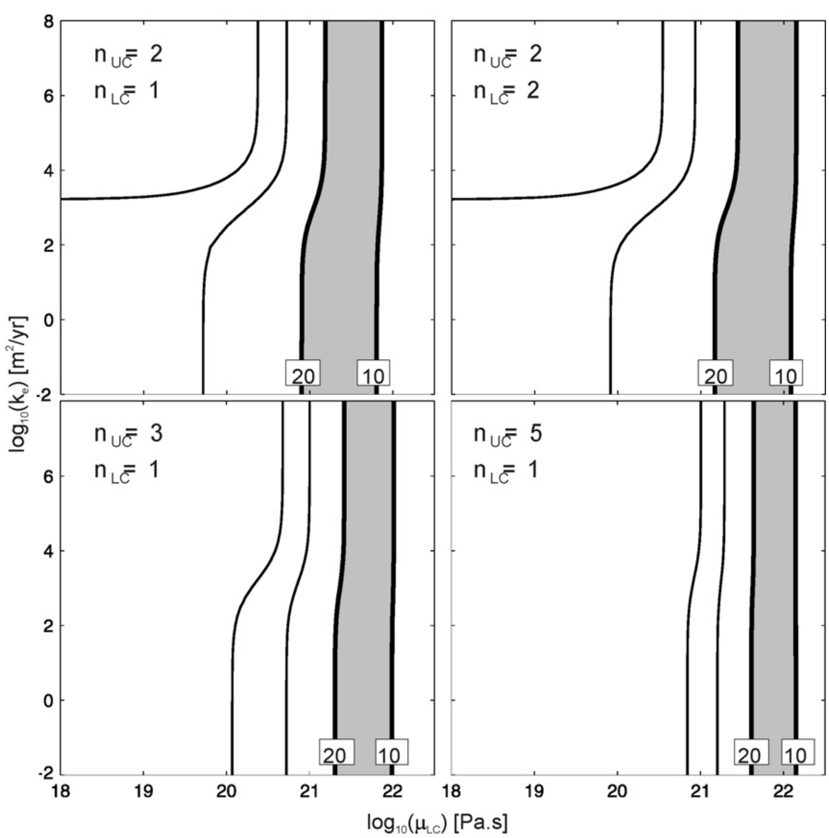

Fig. 14. Effect of changing the power law exponent in the brittle and ductile crust on analytically computed growth rates (with other parameters as in Fig. 13C). Increasing the powerlaw exponent in the brittle layer widens the area with large growth rates.

first order physical processes that govern the process. Schmalholz et al. (2002) considered the stability of a compressed, viscous layer on top of a lower viscous matrix, in absence of erosion. They demonstrated that three modes of deformation occur: matrix folding, detachment folding and gravity folding. For the parameters of our setup, gravity and detachment folding are the two dominant mechanisms. The boundary between detachment and gravity folding is given by (Schmalholz et al., 2002)

$$\frac{q_{\mathrm{grav}}}{q_{\mathrm{det}}} = \left(\frac{3n\mu_{\mathrm{LC}}}{\mu_{\mathrm{UC}}}\right)^{1/3} \frac{4\mu_{\mathrm{UC}}\dot{\varepsilon}_{\mathrm{b}}}{\rho g H_{\mathrm{LC}}}. \tag{12}$$

If $(q_{\mathrm{grav}}/q_{\mathrm{det}}) < 1$, gravity-controlled folding is the dominant mode and vice versa. For the lithospheric parameters employed in this study, $(q_{\mathrm{grav}}/q_{\mathrm{det}}) = 0.1–1$ (with $\mu_{\mathrm{UC}} = 10^{23}$ Pa s, $n = 1$, $\mu_{\mathrm{LC}} = 10^{18}–10^{21}$ Pa s), which thus yields a slight preference for the gravity dominated mode. In this case, the dominant growth rate expression is

$$\frac{q_{\mathrm{grav}}}{\dot{\varepsilon}_{\mathrm{b}}} = \frac{12n\mu_{\mathrm{UC}}\dot{\varepsilon}_{\mathrm{b}}}{\rho g H_{\mathrm{UC}}}. \tag{13}$$

Burg et al. (2004) and Kaus (2005) studied a similar system but with an efficient erosion upper boundary condition and for linear viscous rheologies. For the parameters employed here, their detachment folding mode is relevant, for which the growth rate expression is:

$$\frac{q_{\mathrm{de}}}{\dot{\varepsilon}_{\mathrm{b}}} = 0.86\frac{H_{\mathrm{LC}}}{H_{\mathrm{LC}} + H_{\mathrm{UC}}}\left(\frac{\mu_{\mathrm{UC}}}{\mu_{\mathrm{LC}}}\right)^{1/3}. \tag{14}$$

Evaluating Eqs. (13) and (14), for relevant parameters, yields $q_{\mathrm{de}}/\dot{\varepsilon}_{\mathrm{b}} \sim 2–20$ and $q_{\mathrm{grav}}/\dot{\varepsilon}_{\mathrm{b}} \sim 6$. Since $q/\dot{\varepsilon}_{\mathrm{b}}$ should be larger than ~ 10 for finite amplitude structures to develop, it becomes apparent that erosion dominated folding is, for most parameters, faster than gravity controlled folding, which is why erosion enhances the doming instability.

In simple physical terms, the enhancement of doming through erosion is caused by the removal of weight above the growing, crustal-scale, domes. The dependence of the mechanism on the viscosity of the lower crust is caused by its sensitivity to the viscosity contrast between upper and lower crust.

7. Discussion

In this work we have employed fully coupled visco-elasto-plastic numerical models of upper mantle and crustal-scale deformation to obtain some insight in the processes that may occur when a passive continental margin enters a subduction zone. The models differ from many previous approaches in that they compute mantle flow in a self-consistent manner rather than describe it kinematically, which arguably more closely mimics the Earth. Moreover, they simultaneously incorporate surface processes and allow tracking of time-dependent properties, such as pressure or temperature which facilitates comparison with observation. Whereas these features might make the models more realistic, they also make them more complex and hence computationally more demanding. It therefore remains important to understand to which extent simpler models can be applied to study similar problems.

For this reason we have performed a number of 'technical' simulations in which we studied the effects of changing boundary conditions and rheology. The results indicate that, at least for our setup, viscous deformation is the dominant mechanism and mantle flow is largely insensitive to crustal-scale processes. On the basis of this, there seems to be little reason to question the applicability of mantle convection models with free slip upper boundary conditions. Others, however, have obtained different conclusions. Pysklywec (2006), for example, studied the effects of localized erosion on deep lithospheric structures and showed that significant differences occur if (localized) erosion is present and the mantle–lithosphere is strong. In case of a weaker mantle–lithosphere, the mantle evolution was more similar, even though significant differences occurred on a crustal scale. Whereas it seems that decoupling at a lower crustal level may play a role in explaining the differences, more work is required to quantify these effects.

The models show that crustal-scale deformation is strongly affected by the presence of erosion, consistent with many previous models (Avouac and Burov, 1996; Beaumont et al., 1992; Batt and Braun, 1997). They also illustrate the importance of computing mantle flow in a self-consistent manner since small changes in the subducting or overriding plate rheology or geometry may result in largely different rates of subduction and hence crustal deformation (see e.g. Figs. 3, 5 and 8). In addition, deformation in the crust can be very inhomogeneous for certain setups (e.g. in the dome-exhumation mode), which makes it difficult (but not impossible) to apply thermo-kinematic models.

If the doming/exhumation mechanism, outlined here, is indeed responsible for exhumation processes in the Taiwanese crust, it provides a quantitative mechanism to explain the increased rates of deformation once Taiwan emerged from the sea (Covey, 1986). Subareal erosion rates, namely, are much higher than submarine rates, in particular in the sub-tropical typhoon belt.

We have performed a number of additional simulations, for a slightly different setup, in which the effects of slab breakoff were considered by 'cutting-off' the subducting slab after 10 Myrs of model evolution (Steedman, 2007). As expected, slab-breakoff resulted in isostatic uplift. This uplift occurred however over an area of $\sim$ 1000 km, rather than in a localized area. It does thus not provide a mountain-exhumation mechanisms, at least not for the small-scale mountain-belts studied here. Following slab-breakoff, crustal deformation rates decreased.

In the models presented here, movement of the overriding PSP plate was due to slab pull and ridge push. We have performed a number of additional calculations, for a somewhat different setup, in which the PSP lithosphere was kinematically 'pushed' into the passive continental margin. Whereas the models differ in details, they do not change our conclusions w.r.t. the exhumation modes of the continental crust. This indicates that the most important effect of kinematic pushing is an increase in the background crustal strain rate, and to a lesser extend, the vertical distribution of this strain rate.

One of the most obvious shortcomings of our study is, besides its 2-D nature, the assumption of material dependent and linear creep rheologies. Whereas this simplification greatly reduces the number of model parameters, it is clearly in disagreement with laboratory experiments which show that material properties are strongly temperature dependent (Ranalli, 1995). Whereas a complete study with temperature-dependent rheologies is beyond the scope of this work, we can still obtain some insights by computing effective viscosities for reasonable temperature structures and rock rheologies. The results of such a computation indicate that the existence of a weak lower crust underneath the Taiwanese upper crust is feasible (Fig. 15). Recently, Yamato et al. (submitted for publication) performed a numerical study on the geodynamic evolution of Taiwan, in which they studied a similar setup as ours but with temperature-dependent and nonlinear creep laws. Their best fitting models require both the presence of a weak lower crust and high erosion rates, in full agreement with the analysis presented here. Successful models also feature a dome-like upwelling of the lower crust, although this upwelling is narrower and may occur in an asymmetric fashion.

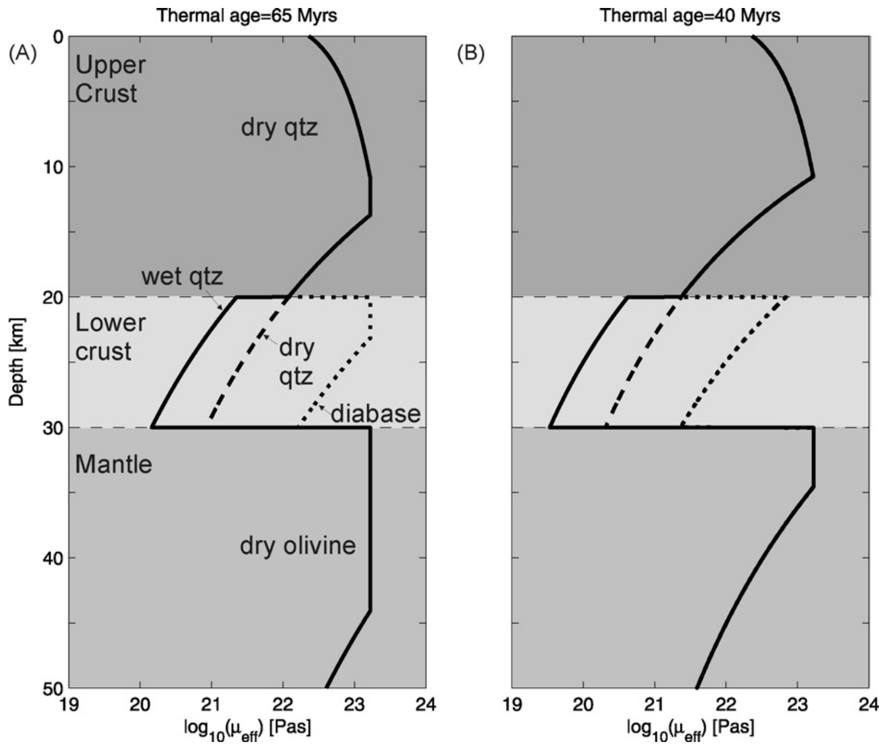

Fig. 15. Effective viscosities as a function of depth for a thermal age of (A) 65 Myrs and (B) 40 Myrs. Effective viscosities are computed for $\dot{\varepsilon}_b = 10^{-15}\,s^{-1}$ from experimentally derived creep laws and the yield stress. Temperature is computed from a plate cooling model. Parameters are: dry quartzite: $A = 2.7 \times 10^{-20}\,Pa^{-2.4}\,s^{-1}$, $E = 156$ kJ/mol, $n = 2.4$ (Ranalli, 1995), wet quartzite: $A = 5.1 \times 10^{-18}\,Pa^{-2.3}\,s^{-1}$, $E = 154$ kJ/mol, $n = 2.3$ (Ranalli, 1995), dry olivine: $A = 4.9 \times 10^{-17}\,Pa^{-3.5}\,s^{-1}$, $E = 535$ kJ/mol, $n = 3.5$ (Hirth and Kohlstedt, 1996), diabase: $A = 3.2 \times 10^{-20}\,Pa^{-3.05}\,s^{-1}$, $E = 276$ kJ/mol, $n = 3.05$ (Carter and Tsenn, 1987). Experimental derived creep laws thus predict, for certain parameters, the existence of a weak lower crust underneath the brittle upper crust.

8. Conclusions

We have employed visco-elasto-plastic coupled mantle–lithosphere models to obtain insights in the dynamics of passive continental margins that enter a subduction zone, a scenario that has been invoked to explain the geodynamic evolution of Taiwan. Results show that, in most cases, the passive margin does not take part in the subduction process. Instead, it decouples from the mantle–lithosphere and deforms in a largely independent manner. The mode of subsequent crustal deformation varies from pure-shear thickening to a dome-like exhumation mode. Cooling and exhumation rates are a strong function of the rheological stratification of the crust: whereas relatively little exhumation of deeper crustal rocks occurs if the crust is homogeneous and strongly coupled to the mantle–lithosphere, much higher rates are obtained if the lower crust is weak and erosion rates are high.

A deeper understanding of the physics of the doming process was obtained by using a semi-analytical perturbation method. Results show that the domal exhumation mode can be attributed to a crustal-scale compressional instability, which is facilitated by erosion and a weaker lower continental crust. The analytical results are confirmed with simplified numerical simulations and are consistent with the findings from lithospheric-scale numerical models.

Computed metamorphic facies, cooling rates and thermo-chronological data are in reasonable agreement with observations in Southern Taiwan, if a dome-like deformation mode occurs in the crust. The presence of an arc in the overriding oceanic lithosphere may increase rates of deformation, but does not dramatically change the overall deformational patterns. If the model is applicable to Taiwan, it suggests that exhumation started before the onset of collision with the Luzon Arc, in agreement with recent thermo-chronological data in Southern Taiwan (Lee et al., 2006). In this scenario, a weak lower crust and high erosion rates are the main contributors to mountain building in Taiwan. This is consistent with recent seismic evidence for decoupling of different crustal levels (Gourley et al., 2007), decreased V_p/V_s (Wu et al., 2007) but increased V_p-velocities and lack of earthquakes (Wu et al., 1997; Gourley et al., 2007) underneath the Central Range region (McIntosh et al., 2005; Wu et al., 2007), as well as with increased rates of exhumation and deformation after the emergence of Taiwan from the sea (Covey, 1986). Recent thermo-kinematic models show that the classical homogeneous critical wedge model is inconsistent with new thermo-chronological data (Simoes et al., 2007; Beyssac et al., 2007). Instead, the authors propose that underplating plays an important role. Our models provide a physical mechanism for this underplating.

The models presented here are simplified in many respects. Although we do not believe that it will change the overall conclusions dramatically, it will still be important to consider the effects of nonlinear and temperature-dependent rheologies in subsequent numerical studies. Moreover, 3-D mantle and crustal flow is likely to play a major role in Taiwan. This requires 3-D numerical techniques capable of computing mantle, lithosphere and surface processes in a self-consistent manner.

Acknowledgements

Computations were conducted at the University of Southern California Center for High Performance Computing and Communications (www.usc.edu/hpcc). We thank John Platt, David Okaya, Francis Wu, Luc Lavier, and Frederic Mouthereau, for stimulating discussions, Sébastien Casteltort for comments on an initial draft of the manuscript, and Dave Stegman, an anonymous reviewer and Mark Jellinek for reviews.

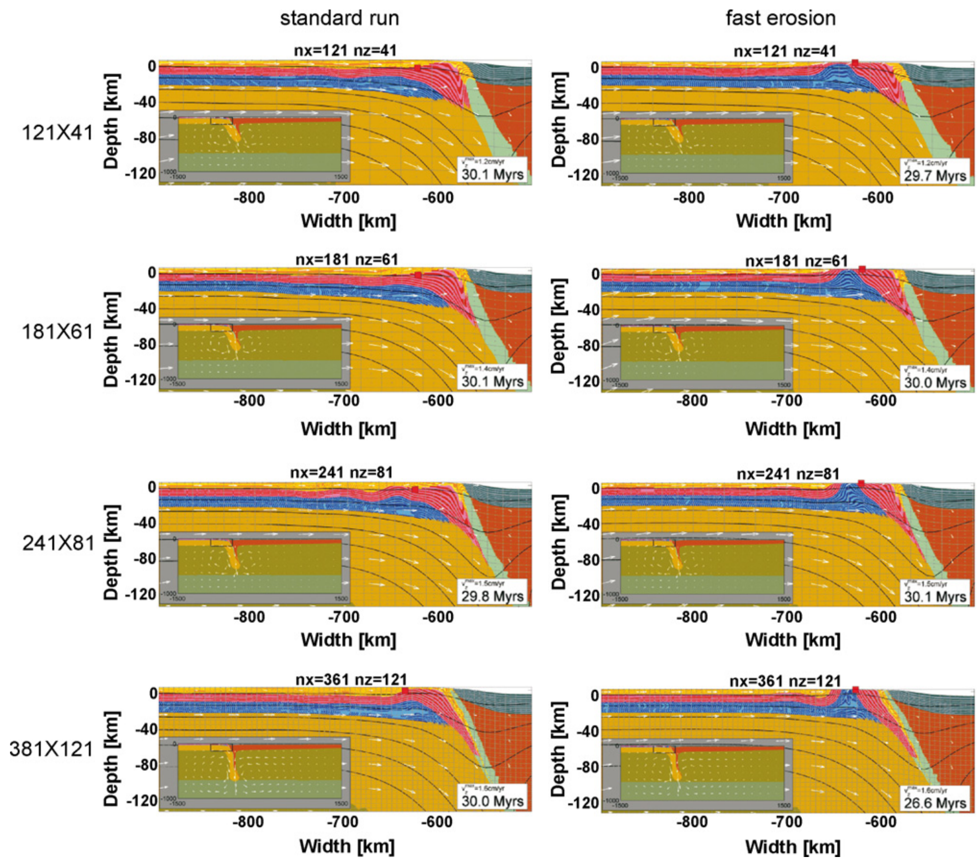

Fig. A.1. Results of a resolution test for both the standard and the fast erosion case. The numerical resolution is increased from 121 × 41 nodes to 381 × 121 nodes (the largest resolution employed in this work). Finite elements, used for computations, are shown in gray (with nodes as dots).

Appendix A. Code verification and resolution test

The code employed in this work has been verified versus a range of analytical solutions that includes 0-D rheology tests (viscous, powerlaw, viscoelastic, viscoelastoplastic), 1-D tests such as the Rayleigh–Taylor instability for viscous of viscoelastic rheologies, the folding instability at infinitesimal and finite amplitudes, diffusion problems and stress around circular inclusions. In addition, the code has successfully been benchmarked versus laboratory experiments and a number of other codes for a brittle extension setup. The simulations described in this work, however, employ a slightly more complex setup which involves subducting slabs. It is thus useful to understand to which extend the overall conclusions of this work depend on the numerical resolutions. For this reason, we have performed a number of simulations in which we varied the resolution from 121 × 41 to 381 × 121 nodes both with the standard model and with a fast erosion setup. The highest resolution is the one employed in this work and is about the maximum that could be performed in a reasonable time with this (serial) version of the code (the use of direct solvers and strong timestep restrictions due to the presence of a free surface makes). The results show that the overall features of the models are captured even at relatively low resolutions (Fig. A.1). Differences, however exists in the rate at which the slab subducts. Interestingly, such differences have also been observed in a recent benchmark study of freesubduction (Schmeling et al. 2008).

References

Avouac, J.P., Burov, E.B., 1996. Erosion as a driving mechanism of intracontinental mountain growth. Journal of Geophysical Research-Solid Earth 101 (B8), 17747–17769.

Barr, T.D., Dahlen, F.A., 1989. Brittle frictional mountain building. 2. Thermal structure and heat budget. Journal of Geophysical Research 94, 3923–3947.

Bassi, G., Bonnin, J., 1988. Rheological modeling and deformation instability of lithosphere under extension. Geophysical Journal 93, 485–504.

Batt, G.E., Braun, J., 1997. On the thermomechanical evolution of compressional orogens. Geophysical Journal International 128, 364–382.

Beaumont, C., Fullsack, P., Hamilton, J., 1992. Erosional control of active compressional orogens. In: McClay, K.R. (Ed.), Thrust Tectonics. Chapman and Hall, New York, pp. 1–18.

Beaumont, C., Jamieson, R.A., Nguyen, M.H., Lee, B., 2001. Himalayan tectonics explained by extrusion of a low-viscosity crustal channel coupled to focused surface denudation. Nature 414 (6865), 738–742.

Beyssac, O., Simoes, M., Avouac, J.P., Farley, K.A., Chen, Y., Chan, Y., Goffé, B., 2007. Late Cenozoic metamorphic evolution and exhumation of Taiwan. Tectonics, doi:10.1029/2006TC002064, TC6001.

Buiter, S.J.H., Babeyko, A.Y., Ellis, S., Gerya, T.V., Kaus, B.J.P., Kellner, A., Schreurs, G., Yamada, Y., 2006. The numerical sandbox: Comparison of model results for a shortening and an extension experiment. In: Buiter, S.J.H., Schreurs, G. (Eds.), Analogue and Numerical Modelling of Crustal-Scale Processes, vol. 253, Geological Society of London Special Publications. Geological Society of London, pp. 29–64.

Burg, J.P., Kaus, B.J.P., Podladchikov, Y., 2004. Dome structures in collision orogens mechanical investigation of the gravity/compression interplay. In: Whitney, D.L., Teyssier, C., Siddoway, C.S. (Eds.), In: Gneiss Domes in Orogeny, Vol. 380. Geological Society of America, Boulder, pp. 47–66.

Burov, E.B., 2003. The upper crust is softer than dry quartzite. Tectonophysics 361 (3–4), 321–326.

Carter, N.L., Tsenn, M.C., 1987. Flow properties of continental lithosphere. Tectonophysics 136, 27–63.

Chai, B.H.T., 1972. Structure and tectonic evolution of Taiwan. American Journal of Science 272, 389–422.

Chemenda, A.I., Yang, R.K., Hsieh, C.-H., Groholsky, A.L., 1997. Evolutionary model for the Taiwan collision based on physical modelling. Tectonophysics 274, 253–274.

Chemenda, A.I., Yang, R.K., Stephan, J.F., Konstantinovskaya, E.A., Ivanov, G.M., 2001. New results from physical modelling of arc-continent collision in Taiwan: evolutionary model. Tectonophysics 333, 159–178.

Conrad, C.P., Hager, B.H., 1999. Effects of plate bending and fault strength at subduction zones on plate dynamics. Journal of Geophysical Research 104, 17551–17571.

Covey, M., 1986. The evolution of foreland basins to steady state: evidence from the western Taiwan foreland basin. In: Allen, P.A., Homewood, P. (Eds.), Foreland Basin. Blackwell, London, pp. 77–90 (Special Publication of the International Association of Sedimentologists).

Cuvelier, C., Segal, A., van Steemhoven, A.A., 1986. Finite element methods and Navier–Stokes equations. In: Mathematics and its Applications. Reidel Publishing Company, Dordrecht.

Dahlen, F.A., Barr, T.D., 1989. Brittle frictional mountain building. 1. Deformation and mechanical energy budget. Journal of Geophysical Research 94, 3906–3922.

Faccenda, M., Gerya, T.V., Chakraborty, S., 2008. Styles of post-subduction collisional orogeny: Influence of convergence velocity, crustal rheology and radiogenic heat production. Lithos 103 (12), 257–287.

Fletcher, R.C., Hallet, B., 1983. Unstable extension of the lithosphere: a mechanical model for Basin-and-Range structure. Journal of Geophysical Research 88 (B9), 7457–7466.

Fuller, C.W., Willett, S.D., Fisher, D., Lu, C.Y., 2006. A thermomechanical wedge model of Taiwan constrained by fission-track thermochronometry. Tectonophysics 425, 1–24.

Goetze, C., Evans, B., 1979. Stress and temperature in the bending lithosphere as constrained by experimental rock mechanics. Geophysical Journal of the Royal Astronomical Society 59, 463–478.

Gourley, J.R., Byrne, T., Chan, Y.-C., Wu, F.T., 2007. Fault geometries illuminated from seismicity in central Taiwan: implications for crustal scale structural boundaries in the northern Central Range. Tectonophysics 445 (3–4), doi:10.1016/j.tecto.2007.08.013.

Hirth, G., Kohlstedt, D.L., 1996. Water in the oceanic upper mantle: implications for rheology, melt extraction and the evolution of the lithosphere. Earth and Planetary Science Letters 144, 93–108.

Hughes, T.J.R., 1987. The Finite Element Method. Dover Publications, New York.

Hutter, K., Jöhnk, K., 2004. Continuum Methods of Physical Modeling. Springer.

Kaus, B.J.P., Becker, T.W., 2007. Effects of elasticity on the Rayleigh–Taylor instability: implications for large-scale geodynamics. Geophysical Journal International 168 (2), 843–862.

Kaus, B.J.P., Podladchikov, Y.Y., 2001. Forward and reverse modeling of the three-dimensional viscous Rayleigh–Taylor instability. Geophysical Research Letters 28 (6), 1095–1098.

Kaus, B.J.P., Podladchikov, Y.Y., 2006. Initiation of localized shear zones in viscoelastoplastic rocks. Journal of Geophysical Research 111 (B04412), doi:10.1029/2005JB003652.

Kaus, B.J.P., 2005. Modelling approaches to geodynamic processes. Ph.d. thesis, Swiss Federal Institute of Technology.

Kaus, B.J.P., Schmalholz, S.M., 2006. 3D Finite amplitude folding: implications for stress evolution during crustal and lithospheric deformation. Geophysical Research Letters 33 (L14309), doi:10.1029/2006GL026341.

Lallemand, S., Font, Y., Bijwaard, H., Kao, M., 2001. New insights on 3-D plate interactions near Taiwan from tomography and tectonic implications. Tectonophysics 335, 229–253.

Lee, Y.-H., Chen, C.-C., Liu, T.-K., Ho, H.-C., Lu, H.-Y., Lo, W., 2006. Mountain building mechanisms in the Southern Central Range of the Taiwan Orogenic Belt from accretionary wedge deformation to arc-continental collision. Earth and Planetary Science Letters 252, 413–422.

Lin, A.T., Watts, A.B., 2002. Origin of the West Taiwan Basin by orogenic loading and flexure of a rifted continental margin. Journal of Geophysical Research 107 (B9), 2185, doi:10.1029/2001JB000669.

Lin, C.H., 2000. Thermal modeling of continental subduction and exhumation constrained by heat flow and seismicity in Taiwan. Tectonophysics 324, 189–201.

Malavieille, J., Lallemand, S., Dominguez, S., Deschamps, A., Lu, C., Liu, C.-S., Schnurle, P., 2002. ACT scientific crew. Arc-continent collision in Taiwan: new marine observations and tectonic evolution. In: Byrne, T., Liu, C.S. (Eds.), In: Geology and Geophysics of an Arc-Continent Collision, vol. 358, pp. 187–211 (Spec. Pap. Geol. Soc. Am.).

McIntosh, K., Nakamura, Y., Wang, T.K., Shih, R.C., Chen, A., Liu, C.S., 2005. Crustal-scale seismic profiles across Taiwan and the western Philippine Sea. Tectonophysics 401 (1–2), 23–54.

Montesi, L.G.J., Zuber, M.T., 2003. Spacing of faults at the scale of the lithosphere and localization instability. 2: Application to the Central Indian Basin. Journal of Geophysical Research 108 (B2), 2111, doi:10.1029/2002JB001924.

Moresi, L., Dufour, F., Muhlhaus, H.-B., 2003. A Lagrangian integration point finite element method for large deformation modeling of viscoelastic geomaterials. Journal of Computational Physics 184, 476–497.

Poliakov, A., Podladchikov, Y., 1992. Diapirism and topography. Geophysical Journal International 109, 553–564.

Pysklywec, R.N., 2006. Surface erosion control on the evolution of the deep lithosphere. Geology 34 (4), 225–228.

Pysklywec, R.N., Beaumont, C., Fullsack, P., 2002. Lithospheric deformation during the early stages of continental collision: numerical experiments and comparison with South Island, New Zealand. Journal of Geophysical Research 107 (B7), 1–19.

Ranalli, G., 1995. Rheology of the Earth, 2nd edition. Chapman and Hall, London.

Ranalli, G., 2003. How soft is the crust? Tectonophysics 361, 319–320.

Regenauer-Lieb, Yuen, D., 2003. Modeling shear zones in geological and planetary sciences: solid- and fluid-thermal-mechanical approaches. Earth-Science Reviews 63, 295–349.

Schmalholz, S.M., 2006. Scaled amplification equation: a key to the folding history of buckled viscous single-layers. Tectonophysics.

Schmalholz, S.M., Podladchikov, Y., 1999. Buckling versus folding: importance of viscoelasticity. Geophysical Research Letters 26 (17), 2641–2644.

Schmalholz, S.M., Podladchikov, Y., Burg, J.P., 2002. Control of folding by gravity and matrix thickness: implications for large-scale folding. Journal of Geophysical Research 107 (B1), doi:10.1029/2001JB000355.

Schmalholz, S.M., Podladchikov, Y., Jamtveit, B., 2005. Structural softening of the lithosphere. Terra Nova 17, 66–72, doi:10.1111/j.1365-3121.2004.00585.x.

Schmalholz, S.M., Podladchikov, Y.Y., 2000. Finite amplitude folding: transition from exponential to layer length controlled growth. Earth and Planetary Science Letters 181 (4), 619–633.

Schmeling, H., Babeyko, A., Enns, A., Faccenna, C., Funiciello, F., Gerya, T., Golabek, G., Grigull, S., Kaus, B.J.P., Morra G., Schmalholz, S., van Hunen, J., 2008. A benchmark comparison of spontaneous subduction models - towards a free surface. Physics of the Earth and Planetary Interiors 171, 198–223.

Schubert, G., Olson, P., Turcotte, D.L., 2001. Mantle Convection in the Earth and Planets. Cambridge University Press.

Sibuet, J.-C., et al., 2002. East Asia plate tectonics since 15 Ma: constraints from the Taiwan region. Tectonophysics 344, 103–134.

Sibuet, J.-C., Hsu, S.-K., 2004. How was Taiwan created? Tectonophysics 379, 159–181.

Simoes, M., Avouac, J.P., Beyssac, O., Goffé, B., Farley, K.A., Chen, Y., 2007. Mountain building in Taiwan: a thermokinematic model. Journal of Geophysical Research 112 (B11405), doi:10.1029/2006JB004824.

Simpson, G.D.H., 2006. How and to what extent does the emergence of orogens above sea level influence their tectonic development? Terra Nova 18 (6), 447–451.

Smith, R.B., 1977. Formation of folds, boudinage and mullions in non-Newtonian materials. Geological Society of America Bulletin 88, 312–320.

Sobolev, S., Babeyko, A., 2005. What drives orogeny in the Andes? Geology 33 (8), 617–620.

Spear, F.S., 1994. Metamorphic Phase Equilibria and Pressure-Temperature-Time Paths. Mineralogical Society of America.

Steedman, C., 2007. Deformation patterns and subduction behavior of continental lithosphere: effects of rheology, surface processes and material parameters. Ms.c. thesis, University of Southern California.

Suppe, J., 1981. Mechanics of mountain-building and metamorphism in Taiwan. Memoir of the Geological Society of China 4, 67–89.

Suppe, J., 1984. Kinematics of arc-continent collision, flipping of subduction, and back-arc spreading near Taiwan. Geological Society of China 6, 21–34.

Suppe, J., 1987. The active Taiwan mountain belt. In: Schaer, J.P., Rodgers, J. (Eds.), The Anatomy of Mountain Ranges. Princenton University Press, Princeton.

Tackley, P., 1996. Effects of strongly variable viscosity on three-dimensional compressible convection in planetary mantles. Journal of Geophysical Research 101 (B2), 3311–3332.

Tao, W.C., O'Connell, R.J., 1992. Ablative subduction: a two-sided alternative to the conventional subduction model. Journal of Geophysical Research 97 (B6), 8877–8904.

Tao, W.C., O'Connell, R.J., 1993. Deformation of a weak subducted slab and variation of seismicity with depth. Nature 361, 626–628.

Teng, L.S., Lee, C.-T., Tsai, Y.-B., Hsiao, L.-Y., 2000. Slab breakoff as a mechanism for flipping of subduction polarity in Taiwan. Geology 28, 155–158.

Turcotte, D.L., Schubert, G., 1982. Geodynamics. Wiley.

van Keken, P.E., King, S.D., Schmeling, H., Christensen, U., Neumeister, D., Doin, M.P., 1997. A comparison of methods for modeling of thermochemical convection. Journal of Geophysical Research 102, 22477–22496.

Wang, Z., Zhao, D.P., Wang, J., Kao, H., 2006. Tomographic evidence for the Eurasian lithosphere subducting beneath south Taiwan. Geophysical Research Letters 33 (18).

Willett, S.D., Fisher, D., Fuller, C., Yeh, E.-C., Lu, C.Y., 2003. Orogen kinematics and erosion rates in Taiwan from thermochronometric data. Geology 31 (11), 945–948.

Winter, J.D., 2000. An Introduction to Igneous and Metamorphic Petrology. Prentice Hall.

Wu, F.T., Rau, R.-J., Salzberg, D., 1997. Taiwan orogeny: thin-skinned or lithospheric collision? Tectonophysics 274, 191–220.

Wu, F.T., 2007. US/Taiwan TAIGER teams, TAIGER (Taiwan Integrated GEodynamics Research) project for testing models of Taiwan orogeny. Geophysical Research Abstracts 9, 02135.

Wu, Y.-M., Chang, C.-H., Zhao, L., Shyu, J.B.H., Chen, Y.-G., Sieh, K., Avouac, J.-P., 2007. Seismic tomography of Taiwan: improved constraints from a dense network of strong motion stations. Journal of Geophysical Research 112, B08312, doi:10.1029/2007JB004983.

Yamato, P., Agard, P., Burov, E., Le Pourhiet, L., Jolivet, L., Tiberi, C., 2007. Burial and exhumation in a subduction wedge: Mutual constraints from thermomechanical modeling and natural *P–T–t* data (Schistes Lustre's, western Alps). Journal of Geophysical Research, 112.

Yamato, P., Mouthereau, F., Burov, E. Taiwan mountain building: insight from 2D thermo-mechanical modeling of a rheologically-stratified lithosphere. Geophysical Journal International, submitted for publication.

Yen, T.P., 1973. Plate tectonics in the Taiwan region. Proceedings of the Geological Society of China 16, 7–21.

Zuber, M.T., 1987. Compression of oceanic lithosphere: an analysis of intraplate deformation in the Central Indian Basin. Journal of Geophysical Research 92 (B6), 4817–4825.